RADIATION FIELDS OF THE LINE SOURCE IN A CYLINDRICAL WIRE GRATING

A THESIS

SUBMITTED TO THE DEPARMENT OF ELECTRICAL AND ELECTRONICS ENGINEERING

AND THE INSTITUTE OF ENGINEERING AND SCIENCE

OF BILKENT UNIVERSITY

IN PARTIAL FULFILLMENT OF THE REQUIREMENTS

FOR THE DEGREE OF

MASTER OF SCIENCE

By

Hakan Karapinar

December 1998

RADIATION FIELDS OF THE LINE SOURCE IN A CYLINDRICAL WIRE GRATING

A THESIS

SUBMITTED TO THE DEPARTMENT OF ELECTRICAL AND

ELECTRONICS ENGINEERING

AND THE INSTITUTE OF ENGINEERING AND SCIENCES

OF BILKENT UNIVERSITY

IN PARTIAL FULFILLMENT OF THE REQUIREMENTS

FOR THE DEGREE OF

MASTER OF SCIENCE

By

Hakan Karapınar

December 1998

I certify that I have read this thesis and that in my opinion it is fully adequate, in scope and in quality, as a thesis for the degree of Master of Science.

Prof. Dr. Ayhan Altıntaş (Supervisor)

I certify that I have read this thesis and that in my opinion it is fully adequate, in scope and in quality, as a thesis for the degree of Master of Science.

Dr. Vladimir Yurchenko(Co-Supervisor)

I certify that I have read this thesis and that in my opinion it is fully adequate, in scope and in quality, as a thesis for the degree of Master of Science.

Assoc. Prof. Dr. Levent Gürel

I certify that I have read this thesis and that in my opinion it is fully adequate, in scope and in quality, as a thesis for the degree of Master of Science.

Assist. Prof. Dr. Birsen Saka

Approved for the Institute of Engineering and Sciences:

Prof. Dr. Mehmet Baray
Director of Institute of Engineering and Sciences

ABSTRACT

RADIATION FIELDS OF THE LINE SOURCE IN A CYLINDRICAL WIRE GRATING

Hakan Karapınar
M.S. in Electrical and Electronics Engineering
Supervisors: Prof. Dr. Ayhan Altıntaş
Dr. Vladimir Yurchenko

December 1998

In this thesis, the transmission effect of a grid structure is analyzed. The grid structure is intended to model the metallic support elements of a radome. The total field for the real and complex position line sources surrounded by the grating structure is obtained in both TM and TE polarizations in the far-field region.

The grid is considered to be a cylindrical array of perfectly conducting cylinders parallel to the z-axis. The radius of each cylinder is small as compared to the wavelength and the length of the cylinders is infinite.
We started with the study of a single perfectly conducting cylinder illuminated by a line source and obtained the formula for the electric and magnetic fields in the far-field region. Then, we calculated far-zone total field for a set of cylinders which form the surface of the radome as a cylindrical periodic grating. The equation for the total electric field in the far-field region is found by using superposition and applying the boundary conditions at the conducting cylinders to find scattering coefficients.

Complex line sources are considered to simulate directed beam fields used in practice. The power pattern and directivity are computed for different parameters of the grating and cylinders. A set of figures is presented to show the relationships between the power pattern, directivity and different parameters of the structure.

Keywords: Grating, directivity, complex source

ÖZET

SİLİNDİRİK IZGARA İÇERİSİNDEKİ BİR ÇUBUK KAYNAĞIN IŞINIMI

Hakan Karapınar
Elektrik ve Elektronik Mühendisliği Bölümü Yüksek Lisans
Tez Yöneticileri: Prof. Dr. Ayhan Altıntaş
Dr. Vladimir Yurchenko
Aralık 1998

Bu tezde, ızgara yapının alan geçirgenliği incelenmiştir. Izgara yapı, metalik elementlerle destekli radomu modellemek için tasarlanmıştır. TM and TE polarizasyonlarında, uzak alan bölgesinde ızgara yapı içerisinde bulunan reel ve karmaşık kaynaklar için toplam elektrik alan çözümleri bulunmuştur.

Izgara, z-eksenine paralel iletken silindirlerden oluşan silindirik dizi olarak düşünülmüştür. Her bir silindirin yarıçapı dalga boyuna göre çok küçük olup, silindirlerin boyları sonsuz olarak alınmıştır. Tek bir silindir ile çalışmaya başlamp bu silindir için toplam elektrik alan formülü elde edildikten sonra, radomun üzerini periodik dizi şeklinde çevreleyen silindirler için toplam elektrik alan formülü bulunmuştur. Uzak alan bölgesindeki her bir silindirin ayrı ayrı oluşturdukları toplam elektrik alan denklemleri süperposisyon kullanılarak bulunup, bu denklemlere, sınır koşulları uygulanarak saçılma katsayıları bulunmuştur.

Pratikte, karmaşık kaynaklar kullanılarak enerjinin yönlendirilmesi simule edilmiştir. Enerjinin yönlendirilmesi ve gücü için tüm veriler, ızgara ve onu oluşturan silindirlerin farklı parametreleri için hesaplanmış ve aralarindaki ilişki bir çok grafik ile gösterilmiştir.

Anahtarkelimeler: Izgara, yönlendirme, karmaşık kaynak.

ACKNOWLEDGMENTS

I would like to express my sincere gratitude to Dr. Ayhan Altıntaş and to Dr. Vladimir Yurchenko for their supervision, guidance, suggestions, encouragement through the development of this thesis.

I would like to thank to Dr. Levent Gürel and to Dr. Birsen Saka for their reading the manuscript and commenting on the thesis.

I would like to thank to my parents, brother and sisters whose understanding made this study possible.

Sincere thanks are also extended to everybody who has helped in the development of this thesis.

Contents

List of Figures

Chapter 1

INTRODUCTION

The problem of scattering from a cylindrical surface has aroused the interest of physicists and engineers for many years because of its large domain of application in optics, acoustics, radiowave propagation and radar techniques [1]. Also, the penetration of electromagnetic waves through a layered system is always an interesting subject of study which finds many applications [2], for instance in evaluating the performance of antennas surrounded by radome. Typically, large radar antennas are covered with radome in order to protect them from weather conditions (rain, wind, sun, etc.) and to enable them to operate continuously without loss of precision.

The design of radomes for antennas may be divided into two separate and relatively distinct classes depending upon whether the antenna is for airborne or ground-based (or ship-based) applications [3]. The airborne radome is characterized by smaller size than ground-based radomes since the antennas that can be carried in an aircraft are generally smaller. The airborne radome must be strong enough to form a part of the aircraft structure and usually must be designed to conform to the aerodynamic shape of the aircraft, missile, or space vehicle in which it is to operate.

A properly designed radome should distort the antenna pattern as little as possible. The presence of a radome can affect the gain, beamwidth, sidelobe level, and the direction of the boresight (pointing direction), as well as change the VSWR and the antenna noise temperature. Sometimes in tracking radars, the rate of the change of the boresight can be important. In this study, we have analyzed how directivity and power pattern of antenna are effected by the grating structure. Here, the source is surrounded by the grating structure. The grating structure is intended to model the metallic support elements of a radome.

In practice, a precise analysis of radome performance is difficult and nearly impossible since the general shape of the radome layer does not fit into the frame suitable for exact analysis. One must therefore resort to some approximate methods. The basic principle of approximation is to find a canonical configuration to approximate the surface of the dielectric layer. A method of modal cylindrical wave spectrum, which is an extension of the plane wave spectrum surface integration technique [4], is applied to the analysis of a two-dimensional elliptic radome. Previously, far-field solutions for complex line source surrounded by a cylindrical dielectric radome are calculated in [2]. The transmission effect of two-dimensional circular radome with periodic gratings is analyzed in [5]. In this thesis, we have obtained far field solutions for real and complex line sources surrounded by a two-dimensional circular radome with periodic conducting cylinders. In this study, we have assumed that, the transmission effect of the dielectric shell is optimized. Thus, we have neglected this effect.

The aim of this thesis is to analyze the effect of the radome formed by a grid of perfectly conducting cylinders on the propagation of the electromagnetic waves, and to obtain how directivity and power change with different radome parameters.

The analysis of the scattering from multiple conducting, dielectric or combination of dielectric and conducting cylinders for incident plane wave is treated by many investigators [6], [7], [8]. However, a rigorous solution to the scattering from conducting cylinders which are placed on the surface of the grating geometry is not available in the literature for real and complex line sources. Here, the solutions for real and complex line sources which are enclosed by grating with conducting cylinders are derived.

The problem of electromagnetic wave scattering from objects are treated using different methods. Among those methods are the integral equation formulation [9], [10], partial differential equation formulation and hybrid techniques which combine the partial differential equation method with a surface integral equation or with an eigenfunction expansion [9]. The integral equation method requires numerical integrations which lead to a system of matrix equations. The order of this matrix equation increases with the electrical dimension and complexity of the scattering objects. This technique requires significant computation time for composite scatterers. On the other hand, to enforce the radiation condition using a partial differential equation method, an approximate absorbing boundary may be used in order to avoid extending the descretized region to infinity. Furthermore, the use of numerical differentiation limits the accuracy of such methods. The hybrid techniques eliminate most of these disadvantages, however, it usually requires more effort in the analytical and numerical implementations [11]. In this thesis, the analysis begins by representing the scattered field of each cylinder as a series expansion in terms of cylindrical functions with unknown coefficients. Then, by applying the boundary conditions on the surface of each cylinder and using superposition to obtain a set of linear equations for unknown scattering coefficients which can be written in a matrix form. The Gaussian elimination with backward substitution method is used to solve these linear equations.

The outline of thesis is as follows. In Chapter 2 we introduce the basic concept of the techniques and the formulation of the problem. In Chapter 3 we introduce the numerical techniques for generating Bessel functions and for solving a set of linear equations. Numerical results are presented in Chapter 4. Main conclusions follow in Chapter 5.

Throughout the analysis, a sinusoidal-varying time dependence e^{jwt} is assumed and suppressed.

Chapter 2

ANALYSIS OF RADIATION THROUGH A RADOME WITH GRATINGS

In this chapter, we obtain the general formulas for radiated electric field due to an electric line source and the total radiated magnetic field due to a magnetic line source inside the multicylindrical structure as it seen in Figure 2.1. The cylinders are assumed to be periodically located over a circle of radius c centered around the source. The radius of each cylinder is a.

Both real and complex line sources are considered. Complex line source is used to simulate a directed beam. The wave field is represented as expansion series of cylindrical waves to evaluate the radiation fields. Then, the effect of transmission through the number of perfectly conducting circular cylinders is found. The surface of many practical scatterers can often be approximated by cylindrical structures [12]. We will consider cylindrical waves for both the real and complex-position line sources surrounded by a set of circular conducting cylinders of infinite length.

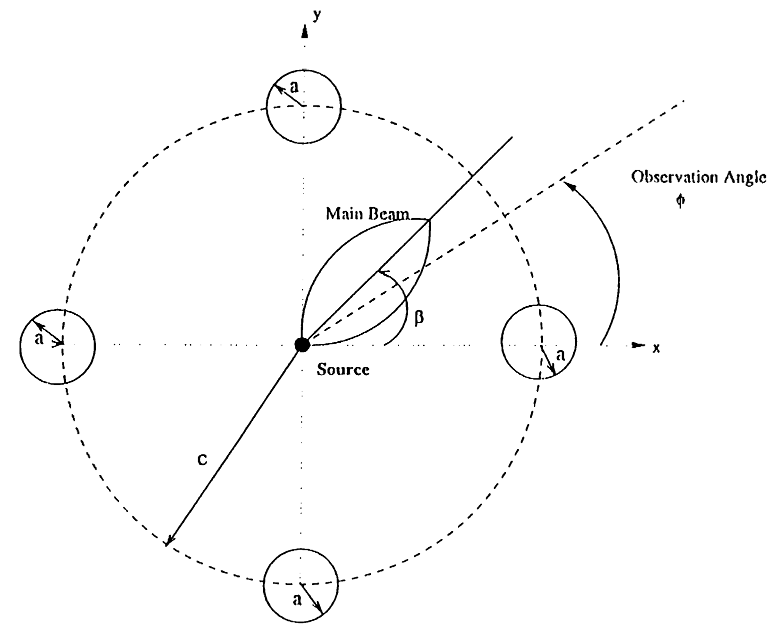

Figure 2.1: Geometry of circular periodic conducting cylinders

Formulation of the problem is initially carried out for a single cylinder with real position electric line source and then extended to the case of multicylindirical structure with real and complex position electric line sources.

2.1 Electric Line Source (TM Polarization) Parallel to Single Cylinder

A line current of infinite length directed along the z axis is assumed to be placed at r' in the vicinity of a circular conducting cylinder as shown in Figure 2.2. The line source is outside the cylinder ($r' > a$).

The cylinder is also assumed to be infinite in length and its axis is parallel to the line source. If the line source of Figure 2.2 is a time-harmonic electric current of constant amplitude I_e, the electric field E_z^{inc} generated everywhere by the source in the free space is found in the following manner.

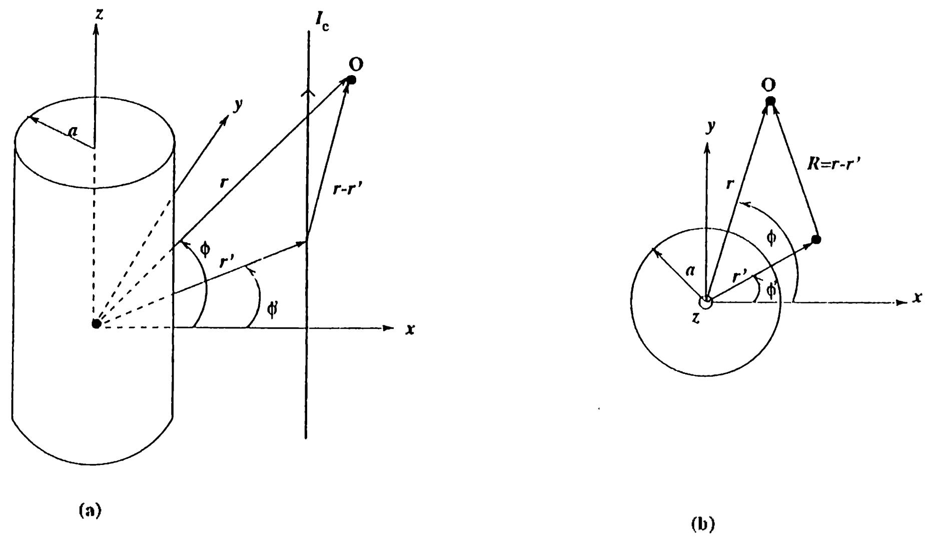

Figure 2.2: Electric line source near a circular cylinder. (a) Side view. (b) Top view

The free space Green's function G of the line source can be written as

$$G(r,\phi;r',\phi') = -\frac{1}{4j}H_0^{(2)}(k_0 \mid \vec{r}-\vec{r'} \mid). \tag{2.1}$$

This is the well-known two-dimensional Green's function for the cylindrical wave [12]. From (2.1), the incident field E_z^{inc} can be found as

$$E_z^{inc} = -\frac{k_0^2 I_e}{4w\epsilon}H_0^{(2)}(k_0 \mid r-r' \mid) \tag{2.2}$$

where $k_0 = 2\pi/\lambda$ is the free space wave number and λ is the wavelength.

By the use of the addition theorem for Hankel functions, we can write (2.2) as

$$E_z^{inc} = -\frac{k_0^2 I_e}{4w\epsilon}\begin{cases} \sum_{n=-\infty}^{\infty} J_n(k_0 r)H_n^{(2)}(k_0 r')e^{jn(\phi-\phi')} & r \le r' \\ \sum_{n=-\infty}^{\infty} J_n(k_0 r')H_n^{(2)}(k_0 r)e^{jn(\phi-\phi')} & r \ge r' \end{cases}. \tag{2.3}$$

In the presence of the cylinder, the total field is composed of two parts: the incident field and the scattered field. The scattered field is produced by the current induced on the surface of the cylinder that acts as a radiator.

The scattered field also has only z component and it can be expressed as

$$E_z^{scat} = -\frac{k_0 I_e}{4w\epsilon}\sum_{n=-\infty}^{\infty} C_n H_n^{(2)}(k_0 r)e^{jn(\phi-\phi')}, \quad a \le r. \tag{2.4}$$

The unknown coefficients C_n can be found by applying the boundary conditions of

$$E_z^{tot}(r = a, 0 \leq \phi \leq 2\pi, z) = 0, \tag{2.5}$$

to the total field on the surface of cylinder

$$E_z^{tot} = E_z^{inc} + E_z^{scat} = 0 \tag{2.6}$$

that yields the equation

$$-\frac{k_0^2 I_e}{4w\epsilon} \sum_{n=-\infty}^{\infty} [J_n(k_0 a) H_n^{(2)}(k_0 r') + C_n H_n^{(2)}(k_0 a)] e^{jn(\phi-\phi')} = 0. \tag{2.7}$$

From here, C_n can be found as

$$C_n = -H_n^{(2)}(k_0 r') \frac{J_n(k_0 a)}{H_n^{(2)}(k_0 a)}, \tag{2.8}$$

which then yields

$$E_z^{tot} = -\frac{k_0^2 I_e}{4w\epsilon} \begin{cases} \sum_{n=-\infty}^{\infty} H_n^{(2)}(k_0 r')[J_n(k_0 r) - \frac{J_n(k_0 a)}{H_n^{(2)}(k_0 a)} H_n^{(2)}(k_0 r)] e^{jn(\phi-\phi')} & r \leq r' \\ \sum_{n=-\infty}^{\infty} H_n^{(2)}(k_0 r)[J_n(k_0 r') - \frac{J_n(k_0 a)}{H_n^{(2)}(k_0 a)} H_n^{(2)}(k_0 r')] e^{jn(\phi-\phi')} & r \geq r' \end{cases} \tag{2.9}$$

For far-field observations ($k_0 r >> 1$) the total electric field of (2.9) can be reduced by replacing the Hankel function $H_n^{(2)}(k_0 r)$ by its asymptotic expression

$$H_n^{(2)}(k_0 r) = \sqrt{\frac{2j}{\pi k_0 r}} j^n e^{-jk_0 r}. \tag{2.10}$$

The total electric field in the far-zone can be expressed as

$$\begin{aligned} E_z^{tot} \simeq -\frac{k_0^2 I_e}{4w\epsilon} \sqrt{\frac{2j}{\pi k_0 r}} e^{-jk_0 r} \sum_{n=-\infty}^{\infty} j^n [J_n(k_0 r') \\ - \frac{J_n(k_0 a)}{H_n^{(2)}(k_0 a)} H_n^{(2)}(k_0 r')] e^{jn(\phi-\phi')} \end{aligned} \tag{2.11}$$

which can be used to compute more conveniently far-field patterns of an electric line source located near a circular conducting cylinder.

2.2 Circular Grating with Many Conducting Cylinders

In this section, we obtain the general formula for the total electric field at the far zone of a multicylindrical structure. In this geometry which is shown in Figure 2.3, the line source is surrounded by the a grating which consists of many perfectly conducting cylinders.

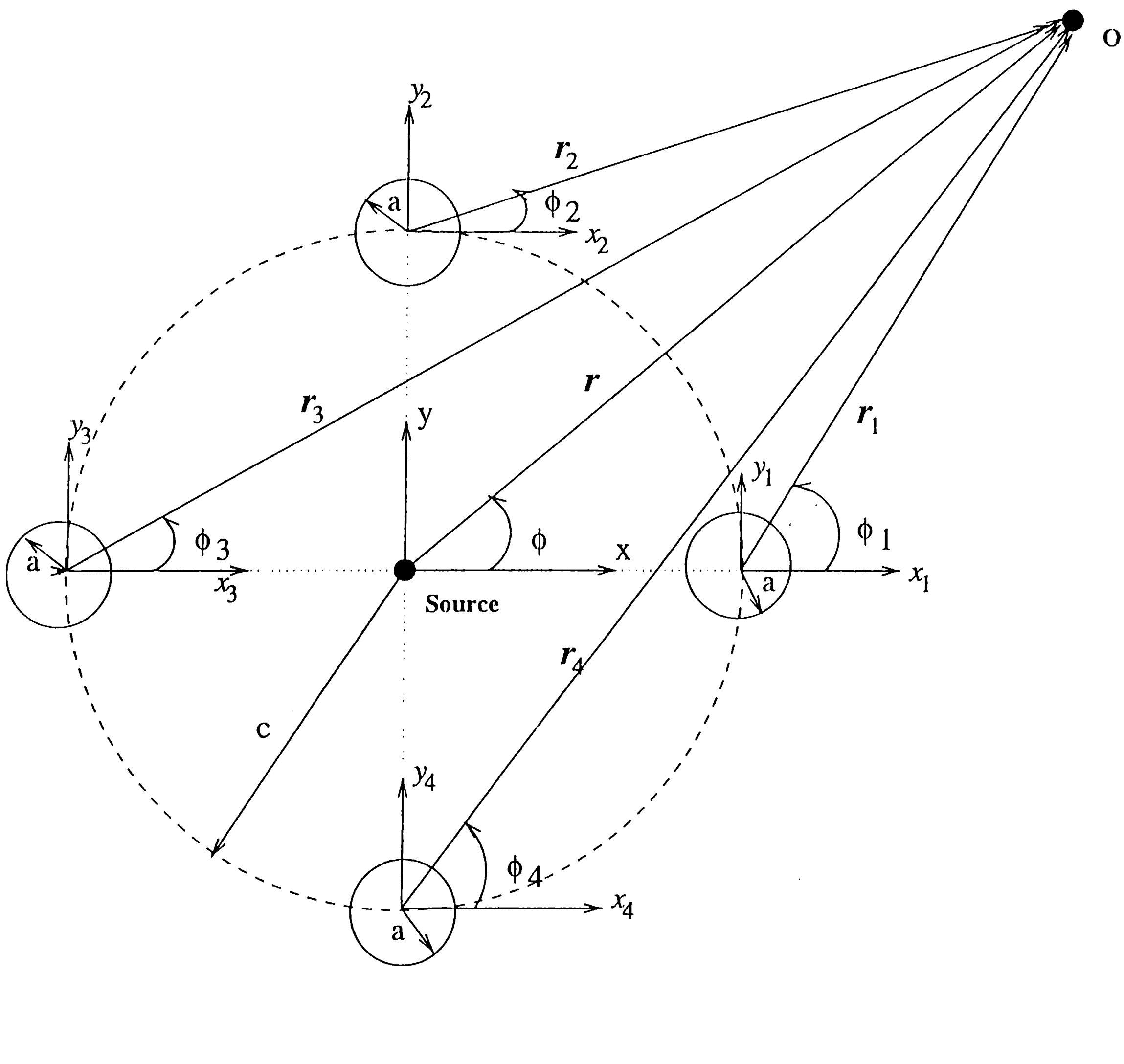

Figure 2.3: The geometry of the circular grating with conducting cylinders.

Here, c is the radius of the grating, a is the radius of the each cylinder, r_i and ϕ_i are the distance and the angle between ith cylinder and observation point for $i = 1...M$, respectively, with M is the total number of cylinders.

For the structure of four cylinders shown in the Figure 2.3, the total field consists of an incident field coming from the source, and of four scattered fields coming from four scatterers:

$$E_z^{tot} = E_z^{inc} + E_{z1}^{scat} + E_{z2}^{scat} + E_{z3}^{scat} + E_{z4}^{scat}. \tag{2.12}$$

The general formula for the total electric field at the observation point for a set of M conducting cylinders on the surface of the radome is [8]

$$E_z^{tot} = E_z^{inc} + \sum_{m=1}^{M} E_{zm}^{scat} \tag{2.13}$$

where

$$E_{zm}^{scat} = -\frac{k_0^2 I_e}{4w\epsilon} \sum_{n=-\infty}^{\infty} C_{mn} H_n^{(2)}(k_0 r_m) e^{jn\phi_m} \tag{2.14}$$

is the corresponding scattered electric field component related to mth cylinder and C_{mn} is the unknown coefficient related to the mth cylinder which includes the effect of all interactions between the cylinders. In the above equations, $J_n(x)$ and $H_n^{(2)}(x)$ are the Bessel and Hankel functions of order n and argument x.

On the surface of the ith cylinder, the boundary conditions are

$$E_{zi}^{inc} + \sum_{m=1}^{M} E_{zm}^{scat} = 0 \quad \text{at } r_i = a, 0 \le \phi_i \le 2\pi \tag{2.15}$$

where a is the radius of each cylinder and M is the total number of cylinders. The first term on the left-hand side of (2.15) represents the incident field at the ith cylinder, in terms of the local coordinates of this cylinder (r_i, ϕ_i). The second term on the left-hand side represents the scattered electric field from all M cylinders in terms of the local coordinates of each individual cylinder (r_m, ϕ_m). In order to solve for the unknown expansion coefficients C_{mn} it is then required to express the scattered field from one cylinder in terms of the local coordinates of another cylinder.

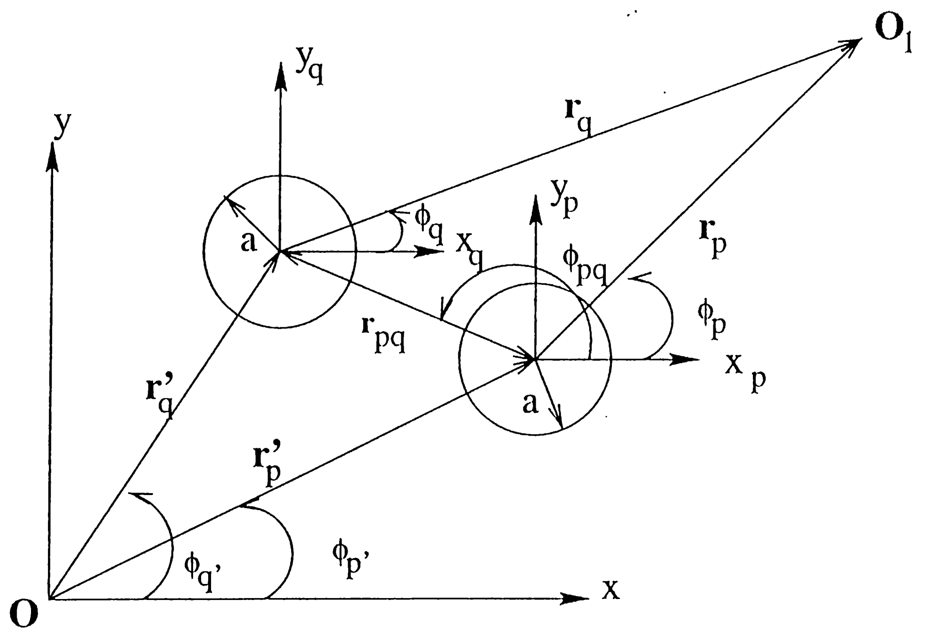

Figure 2.4: Geometry of two circular cylinders and their coordinate systems.

Using the addition theorem for Hankel functions, one can write the transformation from the qth coordinate to the pth coordinate as

$$H_n^{(2)}(k_0 r_q)e^{jn\phi_q} = \sum_{m=-\infty}^{\infty} J_m(k_0 r_p) H_{m-n}^{(2)}(k_0 r_{pq}) e^{jm\phi_p} e^{-j(m-n)\phi_{pq}} \tag{2.16}$$

where $r_{pq} > r_p$ and

$$r_{pq} = \sqrt{r_p'^2 + r_q'^2 - 2r_p' r_q' \cos(\phi_p' - \phi_q')} \tag{2.17}$$

$$\phi_{pq} = cos^{-1}[\frac{r_q' cos\phi_q' - r_p' cos\phi_p'}{r_{pq}}]. \tag{2.18}$$

In the circular grating geometry, $r_q' = r_p' = c$ and $\phi_p' = \frac{2\pi p}{M-1}$ where $p = 0, 1, ..., M-1$ is the cylinder numbers. The transformation from the pth to the qth coordinates is identical to (2.16) except that the p and q should be interchanged. In order to satisfy the boundary conditions as in (2.5), the total electric field component at the mth cylinder is obtained in terms of the local coordinates of the mth cylinder by using the addition theorem in (2.16):

$$E_{zm}^{tot} = E_{zm}^{inc} + E_{zm}^{scat} + \sum_{i=1, i\neq m}^{M} E_{zi}^{scat} \tag{2.19}$$

where

$$E_{zm}^{inc} = -\frac{k_0^2 I_e}{4w\epsilon} \sum_{n=-\infty}^{\infty} J_n(k_0 r_m) H_n^{(2)}(k_0 r_m') e^{jn(\phi_m - \phi')}, \tag{2.20}$$

$$E_{zm}^{scat} = -\frac{k_0^2 I_e}{4w\epsilon} \sum_{n=-\infty}^{\infty} C_{mn} H_n^{(2)}(k_0 r_m) e^{jn\phi_m}, \tag{2.21}$$

$$\sum_{i=1, i\neq m}^{M} E_{zi}^{scat} = B \sum_{i=1, i\neq m}^{M} \sum_{n=-\infty}^{\infty} \sum_{q=-\infty}^{\infty} C_{in} J_q(k_0 r_m) H_{q-n}^{(2)}(k_0 r_{mi}) e^{jq\phi_m} e^{-j(q-n)\phi_{mi}}, \tag{2.22}$$

where
$B = -\frac{k_0^2 I_e}{4w\epsilon}$, $r_{mi} = \sqrt{{r'_m}^2 + {r'_i}^2 - 2r'_m r'_i \cos(\phi'_m - \phi'_i)}$ and
$\phi_{mi} = cos^{-1}[\frac{r'_m cos\phi'_m - r'_i cos\phi'_i}{r_{mi}}]$.

If we apply boundary condition for the mth cylinder

$$E_{zm}^{tot} = E_{zm}^{inc} + E_{zm}^{scat} + \sum_{i=1, i\neq m}^{M} E_{zi}^{scat} = 0 \tag{2.23}$$

with $r_m = a$, $r'_m = c$ and $r'_i = c$ and use the orthogonal property of the exponential function $e^{jn\phi_i}$ we obtain linear equations relating the coefficients C_{mq}:

$$-J_q(k_0 a) H_q^{(2)}(k_0 r_{ms}) e^{-qj\phi_{ms}} = C_{mq} H_q^{(2)}(k_0 a) + \sum_{i=1, i\neq m}^{M} \sum_{n=-\infty}^{\infty} C_{in} J_q(k_0 a) H_{q-n}^{(2)}(k_0 r_{mi}) e^{-j(q-n)\phi_{mi}} \tag{2.24}$$

for $m = 1, ..., M$ and $q = -\infty, ..., -1, 0, 1, ..., \infty$. Where ϕ_{ms} is the angle between line source and mth cylinder, r_{ms} is the distance between mth cylinder and line source, r_{mi} is the distance between ith cylinder and mth cylinder, and ϕ_{mi} is the angle between ith cylinder and mth cylinder.

The set of equations (2.24) can be written as follows:

$$A_i^m = \sum_{h=1}^{M} \sum_{n=-\infty}^{\infty} C_h^n [b_{ih}^{mn}(1 - \delta_{ih}) + d^m \delta_{mn} \delta ih)] \tag{2.25}$$

where δ_{ih} is the Kronecker's delta function

$$\delta_{ih} = \begin{cases} 1 & i = h \\ 0 & i \neq h \end{cases} \tag{2.26}$$

and the elements b_{ih}^{mn}, d_i^m are given, respectively, by

$$b_{ih}^{mn} = H_{m-n}^{(2)}(k_0 r_{ih}) e^{-j(m-n)\phi_{ih}} J_m(k_0 a), \tag{2.27}$$

$$d_i^m = H_m^{(2)}(k_0 a). \tag{2.28}$$

The elements of $\mathbf{A}$ are given by

$$A_i^m = -J_m(k_0 a) H_m^{(2)}(k_0 r_{si}) e^{-jm\phi_{si}} \tag{2.29}$$

and the vector $\mathbf{C}$ represents the unknown expansion coefficients of the scattered field from the M cylinders.

The set of linear equation can be written in the following matrix form

$$\mathbf{A} = \mathbf{SC}, \tag{2.30}$$

or more explicitly

$$\begin{vmatrix} A_1^m \\ \cdot \\ A_i^m \\ \cdot \\ A_M^m \end{vmatrix} = \begin{vmatrix} S_{11}^{mn} & \dots & S_{1h}^{mn} & \dots & S_{1M}^{mn} \\ \cdot & \dots & \cdot & \dots & \cdot \\ S_{i1}^{mn} & \dots & S_{ih}^{mn} & \dots & S_{iM}^{mn} \\ \cdot & \dots & \cdot & \dots & \cdot \\ S_{M1}^{mn} & \dots & S_{mh}^{mn} & \dots & S_{MM}^{mn} \end{vmatrix} \begin{vmatrix} C_1^m \\ \cdot \\ C_i \\ \cdot \\ C_M^m \end{vmatrix} \tag{2.31}$$

where the vectors $\mathbf{A}$ and $\mathbf{C}$ are of dimension $(2N+1)M$, N is the truncation number which has to be chosen so that (2.31) has a convergent solution. The submatrices S_{ih}^{mn} are

$$S_{ih}^{mn} = \begin{cases} b_{ih}^{mn} & i \neq h \ \text{(mutual interaction)} \\ d_i^m \delta_{mn} & i = h \ \text{(self-interaction)} \end{cases} \tag{2.32}$$

where $n, m = -N, ..., -1, 0, 1, ..., N$. The inversion of the matrix S yields the solution for the matrix $\mathbf{C}$.

2.3 Complex Line Source

Complex Source Pulsed Beams (CSPBs) are exact solutions of the wave equation that can be modeled by a time-dependent source located at a complex coordinate point with a proper choice of parameters. These wave fields are confined in beam-like fashion in transverse planes perpendicular to the propagation axis while confinement along the axis is due to temporal windowing. Because they have these properties, CSPBs are useful wave objects for generating and synthesizing highly focused transient fields and for local probing of a medium. Furthermore, as has been shown recently, CSPBs form a new set of basis functions for an exact angular spectrum expansion of source fields [13].

In this thesis, the complex source of time-harmonic line current is considered. The direction, collimation and directivity of the source field is determined essentially by the imaginary displacement of the source coordinate.

Unlike the real line source, the antenna feeders are not uniform in practice. So, to simulate nonuniform radiators the complex line source is used [2]. In Figure 2.5, a complex line source generating a beam is shown.

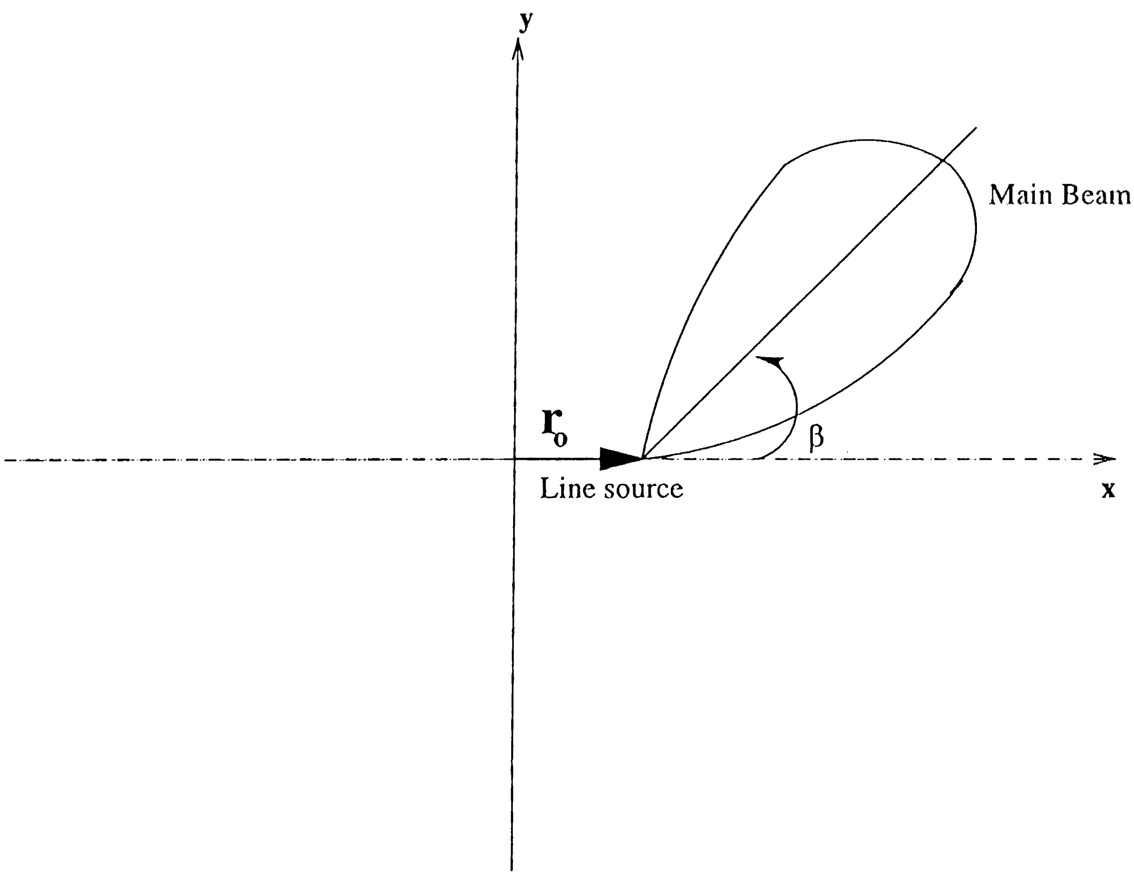

Figure 2.5: Geometry of the complex line source.

The line source is placed at a complex location $\vec{r_s}$ which is given by

$$\vec{r_s} = \vec{r_0} + i\vec{b} = a\hat{x} + ib(cos\beta\hat{x} + sin\beta\hat{y}), \tag{2.33}$$

where the parameter β gives the direction of the beam and b is related to the beam width. For b=0, the source position is real and radiation is axially uniform. Assuming that the source is located at (r_s, ϕ_s), the field intensity at the observation point (r, ϕ) can be written as

$$E_z^{inc} = CH_0^{(2)}(k_0R) = C\sqrt{\frac{2j}{\pi k_0 R}}j^0 e^{jk_0R}. \tag{2.34}$$

for $k_0R >> 1$ where

$$R = \sqrt{r^2 + r_s^2 - 2rr_s cos(\phi - \phi_s)}, \tag{2.35}$$

is the distance of the observation point from the source. $\vec{r_s}$, $\vec{r_0}$ and $\vec{b}$ are the complex source position, real source position and beam parameter vectors given in polar coordinates as $\vec{r_0} = (r_0, \phi_0)$, $\vec{r_s} = (r_s, \phi_s)$ and $\vec{b} = (b, \beta)$. All angles are measured from the x-axis. The values of r_s and ϕ_s are

$$r_s = \sqrt{r_0^2 - b^2 + 2jr_0 bcos\beta}, \tag{2.36}$$

$$\phi_s = cos^{-1}(\frac{r_0 + jbcos\beta}{r_s}). \tag{2.37}$$

In the far field, $R = r - r_s cos(\phi - \phi_s)$ applies in the phase term, $R = r$ in the amplitude term. Substituting R into (2.34), the following expression is obtained.

$$E_z^{inc} = C\frac{e^{jk_0(r - r_0 cos(\phi - \phi_0))}}{\sqrt{k_0 r}}e^{k_0 bcos(\phi - \beta)} \tag{2.38}$$

which yields a maximum at $\phi = \beta$ and a minimum at $\phi = \beta + \pi$.

The incident field can also be written as a series in terms of the addition theorem:

$$E_z^{inc}(r) = C\sum_{n=-\infty}^{\infty} J_n(k_0 r_s)H_n^{(2)}(k_0 r)e^{jn(\phi - \phi_s)}, \quad r \geq r_s. \tag{2.39}$$

When $\vec{b} = 0$, $\vec{r_s} = \vec{r_0}$, the complex line source behaves as a real line source. So, the difference between the formulation of total electric field for real line source and complex line source is only in the incident electric field. The formulations for the scattered fields are the same. Thus, the general formula of total field for M number of cylinders in far field region,

$$E_z^{tot}(r, \phi) = K\sum_{n=-\infty}^{\infty} j^n[J_n(k_0 r_s)e^{jn(\phi - \phi_s)} + \sum_{m=1}^{M} C_{mn}e^{jck_0 Cos(\phi - \phi_m)}e^{jn\phi_m}]. \tag{2.40}$$

where M is the total number of cylinders. ϕ_m is the angle between observation direction and mth cylinder and finally $K = -\frac{k_0^2 I_e}{4w\epsilon}\sqrt{\frac{2j}{\pi k_0 r}}e^{jk_0 r}$.

2.4 Magnetic Line Source (TE Polarization)

Magnetic sources, although not physically realizable, are often used as equivalent source to analyze aperture antennas. If the line source of Figure 2.2 is a magnetic source and it is allowed to recede to the surface of a cylinder ($r' = a$), the total field of the line source in the presence of the cylinder would be representative of a very thin infinite axial slot on the cylinder. If the line source of Figure 2.2 is a magnetic source with current of I_m, the fields that it radiates in the absence of the cylinder can be obtained from those of an electric line source by the use of duality. Doing this we can write the incident magnetic field by referring to H_z^{inc} as

$$H_z^{inc} = -\frac{k_0^2 I_m}{4w\mu} H_0^{(2)}(k_0 \mid r - r' \mid). \tag{2.41}$$

This can also be expressed as

$$H_z^{inc} = -\frac{k_0^2 I_m}{4w\mu} \begin{cases} \sum_{n=-\infty}^{\infty} J_n(k_0 r) H_n^{(2)}(k_0 r') e^{jn(\phi-\phi')} & r \le r' \\ \sum_{n=-\infty}^{\infty} J_n(k_0 r') H_n^{(2)}(k_0 r) e^{jn(\phi-\phi')} & r \ge r' \end{cases}. \tag{2.42}$$

and the scattered magnetic field can be written as

$$H_z^{scat} = -\frac{k_0^2 I_m}{4w\mu} \sum_{n=-\infty}^{\infty} D_n H_n^{(2)}(k_0 r) e^{jn(\phi-\phi')}, \quad a \le r. \tag{2.43}$$

where D_n is used to represent the coefficients of the scattered field. Thus, the total magnetic field

$$H_z^{tot} = H_z^{inc} + H_z^{scat}. \tag{2.44}$$

The corresponding electric field components can be found using Maxwell's equations

$$E_\phi^{tot} = -\frac{1}{jw\epsilon} \frac{\partial H_z^{tot}}{\partial r} \tag{2.45}$$

$$E_\phi^{tot} = -j\frac{k_0 I_m}{4} \begin{cases} \sum_{n=-\infty}^{\infty} [H_n^{(2)}(k_0 r') J_n'(k_0 r) + D_n H_n^{(2)\prime}(k_0 r)] e^{jn(\phi-\phi')} & r \le r' \\ \sum_{n=-\infty}^{\infty} H_n^{(2)\prime}(k_0 r)[J_n(k_0 r') + D_n] e^{jn(\phi-\phi')} & r \ge r' \end{cases} \tag{2.46}$$

where $\frac{\partial J_n(k_0 r)}{\partial r} = J_n'(k_0 r)$ and $\frac{\partial H_n^{(2)}(k_0 r)}{\partial r} = H_n^{(2)\prime}(k_0 r)$.

In order to find unknown coefficients D_n, we apply the boundary condition of

$$E_{\phi}^{tot}(r = a, 0 \leq \phi \leq 2\pi, z) = 0. \tag{2.47}$$

From there, D_n can be found as

$$D_n = -H_n^{(2)}(k_0 r')\frac{J_n(k_0 a)}{H_n^{(2)\prime}(k_0 a)}. \tag{2.48}$$

Thus, the total magnetic field in the far field region can be written as

$$H_z^{tot} \simeq -\frac{k_0^2 I_m}{4w\mu}\sqrt{\frac{2j}{\pi k_0 r}}e^{-jk_0 r}\sum_{n=-\infty}^{\infty} j^n[J_n(k_0 r') - \frac{J_n'(k_0 a)}{H_n^{(2)\prime}(k_0 a)}H_n^{(2)}(k_0 r')]e^{jn(\phi-\phi')}. \tag{2.49}$$

For multicylindrical structure as it seen in Figure 2.1, the total magnetic field

$$H_z^{tot} = H_z^{inc} + \sum_{m=1}^{M} H_{zm}^{scat} \tag{2.50}$$

where

$$H_{zm}^{scat} = -\frac{k_0^2 I_m}{4w\mu}\sum_{n=-\infty}^{\infty} D_{mn}H_n^{(2)}(k_0 r_m)e^{jn\phi_m} \tag{2.51}$$

is the corresponding scattered magnetic field component related to mth cylinder and D_{mn} is the unknown coefficient related to the mth cylinder which includes the effect of all interactions between the cylinders.

The total magnetic field for the mth cylinder is obtained in terms of the local coordinates of the mth cylinder by using the addition theorem in (2.16)

$$H_{zm}^{tot} = H_{zm}^{inc} + H_{zm}^{scat} + \sum_{i=1, i\neq m}^{M} H_{zi}^{scat} \tag{2.52}$$

where

$$H_{zm}^{inc} = -\frac{k_0^2 I_m}{4w\mu}\sum_{n=-\infty}^{\infty} J_n(k_0 r_m)H_n^{(2)}(k_0 r_m')e^{jn(\phi_m-\phi')}, \tag{2.53}$$

$$H_{zm}^{scat} = -\frac{k_0^2 I_m}{4w\mu}\sum_{n=-\infty}^{\infty} D_{mn}H_n^{(2)}(k_0 r_m)e^{jn\phi_m}, \tag{2.54}$$

$$\sum_{i=1,i\neq m}^{M} H_{zi}^{scat} = F \sum_{i=1,i\neq m}^{M} \sum_{n=-\infty}^{\infty} \sum_{q=-\infty}^{\infty} D_{in} J_q(k_0 r_m) H_{q-n}^{(2)}(k_0 r_{mi})$$
$$e^{jq\phi_m} e^{-j(q-n)\phi_{mi}}, \qquad (2.55)$$

where $F = -\frac{k_0^2 I_m}{4w\mu}$, $r_{mi} = \sqrt{r_m'^2 + r_i'^2 - 2r_m' r_i' \cos(\phi_m' - \phi_i')}$ and $\phi_{mi} = cos^{-1}[\frac{r_m' cos\phi_m' - r_i' cos\phi_i'}{r_{mi}}]$.

The corresponding electric field components can be found using Maxwell's equations

$$E_{\phi m}^{tot} = -\frac{1}{jw\epsilon} \frac{\partial H_{zm}^{tot}}{\partial r_m} \qquad (2.56)$$

If we apply boundary condition for mth cylinder,

$$E_{\phi m}^{tot} = E_{\phi m}^{inc} + E_{\phi m}^{scat} + \sum_{i=1,i\neq m}^{M} E_{\phi i}^{scat} = 0 \qquad (2.57)$$

with $r_m = a$, $r_m' = c$ and $r_i' = c$ and use the orthogonal property of the exponential function $e^{jn\phi_i}$ we obtain linear equations relating the coefficients D_{mq}:

$$-J_q'(k_0 a) H_q^{(2)}(k_0 r_{ms}) e^{-qj\phi_{ms}} = D_{mq} H_q^{(2)\prime}(k_0 a)$$
$$+ \sum_{i=1,i\neq m}^{M} \sum_{n=-\infty}^{\infty} D_{in} J_q'(k_0 a) H_{q-n}^{(2)}(k_0 r_{mi}) e^{-j(q-n)\phi_{mi}} \qquad (2.58)$$

for $m = 1, ..., M$ and $q = -\infty, ..., -1, 0, 1, ..., \infty$. here ϕ_{ms} is the angle between line source and mth cylinder,r_{ms} is the distance between mth cylinder and line source, r_{mi} is the distance between ith cylinder and mth cylinder, and ϕ_{mi} is the angle between ith cylinder and mth cylinder. The total magnetic field in the far-field region is computed by using

$$H_z^{tot}(r,\phi) = K \sum_{n=-\infty}^{\infty} j^n [J_n(k_0 r_s) e^{jn(\phi-\phi_s)} + \sum_{m=1}^{M} D_{mn} e^{jck_0 Cos(\phi-\phi_m)} e^{jn\phi_m}].(2.59)$$

where M is the total number of cylinders, ϕ_m is the angle between observation direction and mth cylinder and finally, $K = -\frac{k_0^2 I_m}{4w\mu}\sqrt{\frac{2j}{\pi k_0 r}} e^{jk_0 r}$.

Chapter 3

NUMERICAL METHODS FOR CYLINDRICAL FUNCTIONS AND LINEAR EQUATIONS

3.1 Computation of Bessel and Hankel Functions

In this chapter, the numerical computation of Bessel and Hankel functions of the first and the second kind for integer orders and complex arguments are considered. The numerical computation of linear equation ($Ax = b$) is solved by using Gaussian elimination with backward substitution. The algorithm for Bessel functions makes use of backward recurrence for the computation of Bessel functions of the first kind where applicable, and of Hankel's asymptotic expansion for large arguments.

Bessel functions of integer order are the natural and general solutions of many radiation, scattering and guided wave problems which are formulated in the cylindrical coordinate system. Bessel functions are also used in the mathematical description of numerous physical phenomena besides electromagnetism. Consequently, their accurate computation is of general importance.

$J_n(z)$ and $Y_n(z)$, Bessel function of the first and second kind respectively are solutions to Bessel's differential equation

$$z^2y'' + zy' + (z^2 - n^2)y = 0 \tag{3.1}$$

In this thesis, we generate Bessel functions using the subroutine developed by Anil Bircan [2] following the algorithm presented by Du Toit [14]. In this method, forward and backward iterations are used to compute $J_n(z)$ and $Y_n(z)$ based on the recurrence relation

$$B_{n+1}(z) = \frac{2n}{z}B_n(z) - B_{n-1}(z) \tag{3.2}$$

for all orders for a given argument z. From this relation, if $B_n(z)$ and $B_{n-1}(z)$ are known $B_{n+1}(z)$ is found with increasing N (forward recurrence), if $B_n(z)$ and $B_{n+1}(z)$ is known, $B_{n-1}(z)$ are calculated with decreasing N (backward recurrence).

Before using this relation, the stability of recurrence should be guaranteed. Any round-off error will be amplified by the factor $2n/z$, and accumulation of these errors occur with the repetitive use of (3.2). The relative error are, however, decreasing when the functions B_n are increasing in the process of iteration. So, progressing through increasing value of $|B_n(z)|$ appears to be the best strategy.

Therefore, for $J_n(z)$ functions, the backward recurrence is stable since $|J_n(z)|$ are increasing rapidly with decreasing n. For $Y_n(z)$, when z is complex, the backward recurrence is stable for small n but the forward recurrence is needed for $n > r$ where r is the index corresponding to the minimum of $|Y_n(z)|$.

From the Figures (3.1) and (3.2), when z is real or when $|Re(z)| >> |Im(z)|$, general magnitude of $J_n(z)$ and $Y_n(z)$ for a given argument z is approximately constant for $n < |z|$, but for $n > |z|$, $Y_n(z)$ increases with increasing n and $J_n(z)$ increases with decreasing n. So, all higher orders of $Y_n(z)$ can be computed from $Y_0(z)$ and $Y_1(z)$ by using forward recurrence. All lower orders of $J_n(z)$ can be computed from $J_{q+1}(z)$, $J_q(z)$ which are arbitrary initialized by using backward recurrence.

When z is complex, the same rule still applies for $J_n(z)$ since it decreases with increasing n for all values of n. $Y_n(z)$ can be calculated from $Y_r(z), Y_{r+1}(z)$ using forward recurrence for $n > r$ and backward recurrence for $n < r$ where r is the value of n to yield a minimum to $Y_n(z)$ for a given argument z.

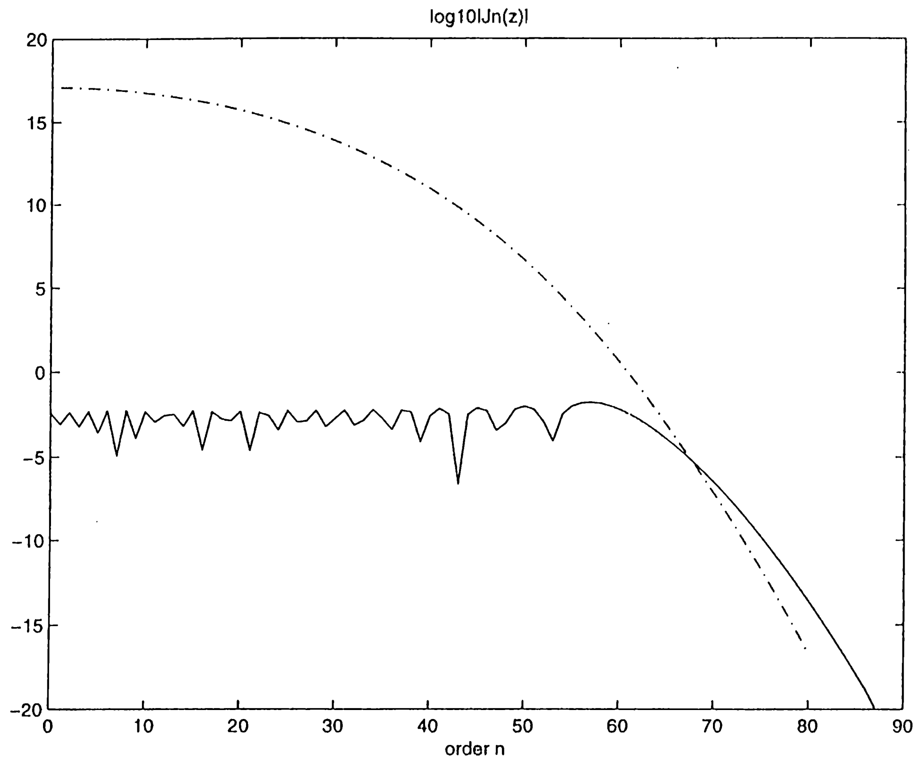

Figure 3.1: $|J_n(z)|$, Argument: z=60 solid line, z=50+20i dash-dotted line

The algorithm of $J_n(z)$ is started with estimating of the starting point for backward recurrence. The minimum value for q (the starting point for backward recurrence) is found in [2] as

$$q_{min} \approx \begin{cases} |z| + 10.26|z|^{0.341015} + 1.8, & |z| \leq 25 \\ |z| + 6.6362|z|^{0.342481} + 0.4, & |z| > 25. \end{cases} \tag{3.3}$$

After finding q_{min} the normalized constant S is computed. Since $J_n(z)$ is obtained by normalization of $B_n(z)$

$$J_n(z) = \frac{B_n(z)}{S} \tag{3.4}$$

S is computed in [2] as

$$S = B_0(z) + 2\sum_{k=1}^{q/2} B_{2k}(z) \tag{3.5}$$

when $Im(z) < 1$ and

$$S = B_0(z) + 2\sum_{k=1}^{q/2} (-1)^k B_{2k}(z) \tag{3.6}$$

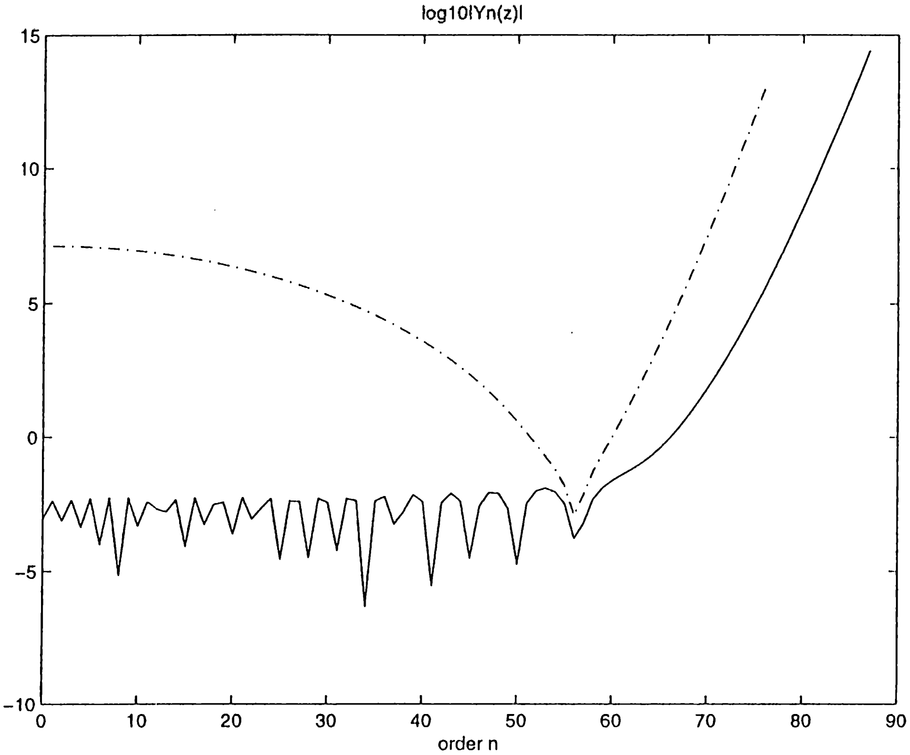

Figure 3.2: $|Y_n(z)|$, Argument: z=60 solid line, z=50+20i dash-dotted line

when $Im[z] > 1$. After computing S, $J_n(z)$ is calculated by using (3.4).

The algorithm of computing $Y_n(z)$ is started by using Neumann's expansion

$$Y_0(z) = \frac{2}{\pi}[(ln(z/2) + \tau)J_0(z) - 2\sum_{k=0}^{\infty}(-1)^k \frac{J_{2k}(z)}{k}], \tag{3.7}$$

$$Y_1(z) = \frac{2}{\pi}[(ln(z/2) + \tau - 1)J_1(z) - \frac{J_0(z)}{z} - \sum_{k=1}^{\infty}(-1)^k \frac{2k + J_{2k+1}(z)}{k(k+1)}]. \tag{3.8}$$

for calculating $Y_0(z)$ and $Y_1(z)$ using forward recurrence when z is real or when $N < |z|$ if z is complex. But, when z is complex and $N > |z|$, $Y_n(z)$ can be calculated from $Y_r(z)$ and $Y_{r+1}(z)$ using backward recurrence. In [2], r is calculated as $r = [|z| + |Im(z)|/2]$ (this can be verified in Figure 3.2).

$Y_r(z)$ and $Y_{r+1}(z)$ can be determined from $Y_0(z)$, $Y_1(z)$ and the $J_n(z)$ functions for $N < |z|$ by using the expansion of the recurrence relation (3.2), in [2]

$$B_0(z) = P_{11}(r,z)B_r(z) + P_{12}(r,z)B_{r+1}(z), \tag{3.9}$$

$$B_1(z) = P_{21}(r,z)B_r(z) + P_{22}(r,z)B_{r+1}(z). \tag{3.10}$$

By using the Wronskian

$$J_{n+1}(z)Y_n(z) - J_n(z)Y_{n+1}(z) = \frac{2}{\pi z}, \tag{3.11}$$

and the fact that determinant of the P matrix is unity, $\det(P)$=1, $P_{11}(r,z)$, $P_{12}(r,z)$, $P_{21}(r,z)$ and $P_{22}(r,z)$ are calculated.

After these, $Y_r(z)$ and $Y_{r+1}(z)$ are computed by using

$$Y_r(z) = \frac{1}{J_0(z)}[J_r(z)Y_0(z) + \frac{2p_{12}}{\pi z}], \tag{3.12}$$

$$Y_{r+1}(z) = \frac{1}{J_0(z)}[J_{r+1}(z)Y_0(z) + \frac{2p_{11}}{\pi z}]. \tag{3.13}$$

So, with r, $Y_r(z)$ and Y_{r+1}, $Y_n(z)$ is produced by backward recurrence for $n < r$ and by forward recurrence for $n > r$.

The accuracy of the algorithms was also tested by examining the numerical error in the Wronskian

$$error = J_{n+1}(z)Y_n(z) - J_n(z)Y_{n+1}(z) - \frac{2}{\pi z}. \tag{3.14}$$

For illustration, this error is divided by $|J_{n+1}(z)| + |J_n(z)|$,

$$|\epsilon| = \frac{J_{n+1}(z)Y_n(z) - J_n(z)Y_{n+1}(z) - (2/\pi z)|}{|J_{n+1}(z)| + |J_n(z)|} \tag{3.15}$$

The relative error $|\epsilon|$ is representative in all four functions involved.

The result follows when it is assumed that the relative errors in all four functions involved have the same amplitude, but are uncorrelated. This error $|\epsilon|$, $J_n(z)$ and $Y_n(z)$ for z=120+10i are depicted in figure. The relative error is in the order of $10^{-15}, 10^{-16}$ which compares favorably with the double precision used in the codes.

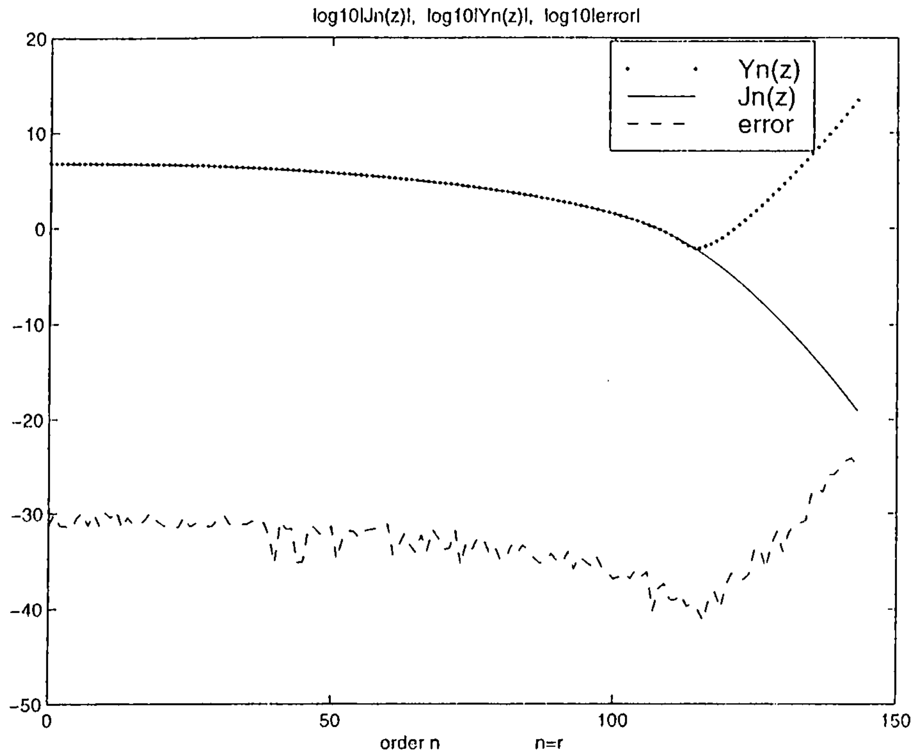

Figure 3.3: —RelativeError—

3.2 Solution of Linear Equations

A system of n linear equations in n unknown is usually expressed in the general form as follow:

$$\begin{aligned} a_{11}x_1 + a_{12}x_2 + \ldots a_{1n}x_n &= b_1 \\ a_{21}x_1 + a_{22}x_2 + \ldots a_{2n}x_n &= b_2 \\ &. \\ &. \\ &. \\ a_{n1}x_1 + a_{n2}x_2 + \ldots a_{nn}x_n &= b_n. \end{aligned} \tag{3.16}$$

The coefficients $a_{11}, a_{12}, \ldots, a_{nn}$ are assumed to be floating point numbers as are the right-hand sides $b_1, b_2, \ldots, b_n$. The problem is to find numbers $x_1, x_2, \ldots, x_n$ so that each of the equations in (3.16) is satisfied. Often it is convenient to express (3.16) by using matrix-vector notation. That is, we can write

$$Ax = b \tag{3.17}$$

where A is the $n \times n$ matrix.

Slightly more general and also useful is the uppertriangular form of the system (3.16) in which $a_{ij} = 0$ if $i > j$. That is, the coefficient matrix has the form

$$\begin{pmatrix} a_{11} & a_{12} & \cdot & \cdot & \cdot & a_{1n} \\ 0 & a_{22} & \cdot & \cdot & \cdot & a_{2n} \\ \cdot & & & & & \\ \cdot & & & & & \\ \cdot & & & & & \\ 0 & & & & 0 & a_{nn} \end{pmatrix}. \tag{3.18}$$

In this case, the equations are as follows

$$\begin{aligned} a_{11}x_1 + a_{12}x_2 + a_{13}x_3 + \ldots a_{1n}x_n &= b_1 \\ a_{22}x_2 + a_{23}x_3 + \ldots a_{2n}x_n &= b_2 \\ &\cdot \\ &\cdot \\ &\cdot \\ a_{n-1,n-1}x_{n-1} + a_{n-1,n}x_n &= b_{n-1} \\ a_{nn}x_n &= b_n. \end{aligned} \tag{3.19}$$

The solution to such a system is easily determined by backsubstituting. That is, the last equation is solved for x_n ,

$$x_n = b_n/a_{nn}, \tag{3.20}$$

then this value is used in the next to last equation to determine x_{n-1} ,

$$x_{n-1} = (b_{n-1} - a_{n-1,n}x_n)/a_{n-1,n-1}, \tag{3.21}$$

which in turn is used in the $(n-2)nd$ equation to determine x_{n-2} , etc.

3.2.1 Elimination Method

The first method for the solution of equations is just an extension of the familiar method of eliminating one unknown between a pair of simultaneous equations. It is generally called Gaussian elimination and is the basic pattern of a large number of methods that can be classed as direct methods.

3.2.2 Gaussian Elimination

The most frequently used method for solving moderately sized linear systems is also one of the oldest such methods, namely, Gaussian elimination.

The idea of Gaussian elimination is to transform a linear system of the general form (3.16) into a system of the special upper triangular form(3.18). The solution is then found directly by backsubstitution. The transformation can be done in such a way that, if exact arithmetic is used, the solution of the triangular system will be the same as the solution to the original system. Of course, computationally the transformation will involve rounding errors. Hence the transformed system will have a solution that may differ somewhat from the solution to the given system. Note, however, that the only error is due to rounding, that is, there is no truncation error in this method.

The transformation referred to above is actually a series of transformation in which the coefficients in the lower part of the system are systematically replaced by zeros. First of all, note that the following elementary operations on the system (3.16) have no effect on the solution of the system:

(i) An equation can be multiplied by a nonzero constant. That is, each coefficient end the right-hand side can be multiplied by the same nonzero number.

(ii) Two equations can be added together and either of the equations replaced by the sum.

(iii) Two equations can be interchanged. That is, the equations can be written down in any order.

To verify that (i) has no effect on the solution is trivial since such an operation really does not change the equation. Also it is clear that (iii) has no effect on the solution. Operation (ii), however, is not quite so simple.

To solve a system of linear equations,

1. Augment the $n \times n$ coefficient matrix with the vector of right-hand sides form a $n \times (n+1)$ matrix.

2. Interchange rows if necessary to make the value of a_{11} the largest magnitude of any coefficient in the first column.

3. Create zeros in the second through nth rows in the first column by subtracting a_{i1}/a_{11} times the first row from the ith row. Store the a_{i1}/a_{11} in a_{i1} $i = 2, ..., n$.

4. Repeat steps (2) and (3) for the second through the $(n-1)$st rows, putting the largest-magnitude coefficient on the diagonal by interchanging rows (considering only rows j to n), and then subtracting a_{ij}/a_{jj} times the jth row from the ith row so as to create zeros in all positions of the jth column below the diagonal. Store the a_{ij}/a_{jj} in a_{ij}, $i = j+1, ..., n$. At the conclusion of this step, the system is upper-triangular.

5. Solve for x_n from the nth equation by

$$x_n = a_{n,n+1}/a_{nn}. \tag{3.22}$$

6. Solve for $x_{n-1}, x_{n-2}, \cdots, x_1$ from the $(n-1)$st through the first equation in turn, by

$$x_i = \frac{a_{i,n-1} - \sum_{j=i+1}^{n} a_{ij} x_j}{a_{ii}}. \tag{3.23}$$

In this thesis, the linear equations of the total electric field for each cylinder are obtained by applying boundary conditions on the surface of the each cylinder.

We have used this method to solve linear equations in matrix form in (2.36).

Chapter 4

NUMERICAL RESULTS AND DISCUSSION

As mentioned in Chapter 1, the aim of this study is to analyze the effect of a circular grating which consists of an array of conducting cylinders on the transmission of electromagnetic fields radiated by a real or complex line source placed inside this structure for both E and H polarization.
In our investigation, we are interested in periodic conducting cylinders. In this chapter, numerical results for two polarizations (E and H polarizations) are obtained. For these two cases, the subject is discussed in terms of normalized power pattern and the directivity which represent two important parameters in design problem.

4.1 Normalized Power Pattern

In this section, we have analyzed normalized power pattern. The associated formula for the normalized power pattern is given as

$$P_{Norm} = \frac{|U^{tot}(r,\phi)|^2}{|U^{tot}_{max}(r,\phi)|^2} \tag{4.1}$$

where $U^{tot} = E_z^{tot}$ for E polarization and $U^{tot} = H_z^{tot}$ for H polarization.
For far field region the total field is obtained as

$$U^{tot}(r,\phi) = K \sum_{n=-\infty}^{\infty} j^n [J_n(k_0 r_s) e^{jn(\phi-\phi_s)} + \sum_{m=1}^{M} T_{mn} e^{jck_0 cos(\phi-\phi_m)} e^{jn\phi_m}] \quad (4.2)$$

where $T_{mn} = C_{mn}$ for E polarization and $T_{mn} = D_{mn}$ for H polarization, M is the total number of cylinders, ϕ_m is the angle between observation direction and mth cylinder, $K = -\frac{k_0^2 I_e}{4w\epsilon}\sqrt{\frac{2j}{\pi k_0 r}} j^0 e^{jk_0 r}$.

4.1.1 *E* Polarization

In order to observe the effect of conducting cylinders on the radiation of the far-field, we have examined power pattern of the source. In the power pattern, normalized power is changed with observation angle ϕ. In this chapter, normalized power is plotted as a function of observation angle for different parameters of the structure and sources. The number of cylinders are shown by M and N is the truncation number. We have started to compute power pattern for the case of no interaction between cylinders. Then, we have included mutual interaction between cylinders. One of the advantages of the proposed method is the possibility of computing the power pattern of the field scattered by many cylinders including all mutual interactions between the cylinders or without interactions by simply setting all the elements in the off-diagonal submatrices to zero. The interaction component of the scattered field is an important quantity in the multiple scattering. To illustrate the effect of mutual interaction on the total field pattern, Figure (4.1) and Figure (4.2) are plotted. They show the power of four and six identical conducting cylinders each of radius 0.0064λ (ka=0.4) which are located symmetrically with respect to x and y-axes and excited by a complex source. The parameters are $ka = 0.4$, $kb = 5$ which corresponds to a beam width of 42^0, radome radius (c) of 10λ, $\beta = 0$ means beam is directed toward cylinder. From these figures, we can say that the scattered field due to the interaction between cylinders must be considered since it causes a discrepancy of 5 to 10 dB especially in the side lobe regions.

Figure (4.3) shows how the power pattern of the real line source changes with the observation angle (ϕ). For a real line source, the directivity of the antenna is unity, because the real line source radiates energy uniformly in all directions. Because of the symmetric geometry, the total field is a periodic function of angle ϕ whose period depends on the number of cylinders. The field is scattered more with increasing the number of cylinders. We are interested in complex line source more than in real line source since the former is a directional source and directivity is an important parameter of the antenna.

For a complex line source, the directivity is greater than one ($D > 1$). The incident field changes with angle ϕ as $E_z^{inc} = Ce^{k_0 b cos(\phi-\beta)}$ which yields a maximum at $\phi = \beta$ and a minimum at $\phi = \beta + \pi$ as it seen in Figure 4.4. This figure shows the effect of cylinders on radiation of electric field. If the source is in free space (absence of cylinders), amplitude of electric field is maximum at the beam direction and minimum at the opposite direction. If the source is placed between two cylinders, the main beam is distorted and decreased. At the same time, the backscattered field is created by the scatterers.

The truncation number (N) shows how many terms in the series (4.2) are needed to obtain convergence. The truncation number required to obtain a specified accuracy depends on the parameters ka and kc. As the radius of the cylinders increases, more terms are needed. However, for very small cylinder radius ($a \ll \lambda$) which is used in this study, the first nine terms ($N = 4$) are sufficient to obtain convergence for $kc = 62.8$. The Figures 4.5, 4.6 and 4.7 illustrate this result.

In order to show how power pattern is effected by the total number of cylinders (M), we have plotted Figures 4.8 through 4.11 for a grating consisting of two, four, six and ten cylinders with $ka = 0.4$, $kb = 5$, $kc = 62.8$, $\beta = 0$, $N = 5$ and $r_0 = 0$ (source is in the center of the grating). From these figures, we can see that the main beam is distorted more with increasing the number of cylinders. At the same time, the sidelobes and backlobes of the beam are increased with increasing the number of cylinders as well which is mainly due to the contribution of each cylinder to the scattered field.

The power pattern is dependent on the structure parameters. This dependence is presented in Figures 4.12, 4.13, 4.14 for grating consisting of four cylinders. In these figures, the power pattern is obtained for different radii of grating and cylinders. As observed in these figures, the distortion of the main beam and backscattered field are increased with increasing cylinders radius and decreasing radome radius. Because, when we decrease radome radius and increase cylinders radius the interactions between source and cylinders increase.

The effects of the beam parameters on the power pattern are observed in Figures 4.15 and 4.16. From these figures, we can say that the sidelobes and backlobes of the beam are decreased with increasing beam width and with choosing beam direction between two cylinders. If we do these, the distortions of the main beam are decreased.

4.1.2 *H* Polarization

In this section, we have analyzed magnetic field and power pattern of magnetic line source. The power pattern of magnetic line source (H polarization) is similar to the power pattern of electric line source (E polarization). Thus, we have not explained figures for H polarization in detail. We have compared E and H polarization in this section.

The effect of cylinders on the magnetic field is shown in Figure 4.17. In this figures, the total magnetic field is plotted for two cases. First case, the source is in free space without any cylinder. In this case, the field is maximum when $\phi = \beta$ (where $\beta = 0$) and zero when $\phi = \beta + \pi$. Second case, the source is in between two cylinders. In this case, the scattered field is created due to conducting cylinders. The cylinders create backscattered field. Figure 4.18, 4.19 and 4.20 present power pattern for different truncation numbers and for different number of cylinders. From these figures, we can see that, the truncation number N equal to four is sufficient to calculate field correctly for $ka = 0.4$, $kb = 5$, $kc = 62,8$ and $M = 2,4,6$. The total number of cylinders do not affect the main beam, but it affects the backscattered field. If we increase the number of cylinders, the ripple of backscattered field increases mainly due to the number of cylinders at the backward direction of beam increase. The effect of cylinder radius is examined in Figure 4.21. If we increase cylinder radius, the backlobes level increases due to the interactions between source and cylinders.

If we compare the results of E and H polarizations, from the Figures 4.4, 4.5, 4.6, 4.7 and Figures 4.17, 4.18, 4.19, 4.20 we can say that, the effects of the conducting cylinder in E polarization is greater than the effects of cylinders in H polarization. Because, power pattern in H polarization is more sensitive to the size of cylinder than power pattern in E polarization as seen from Figure 4.13 and Figure 4.21.

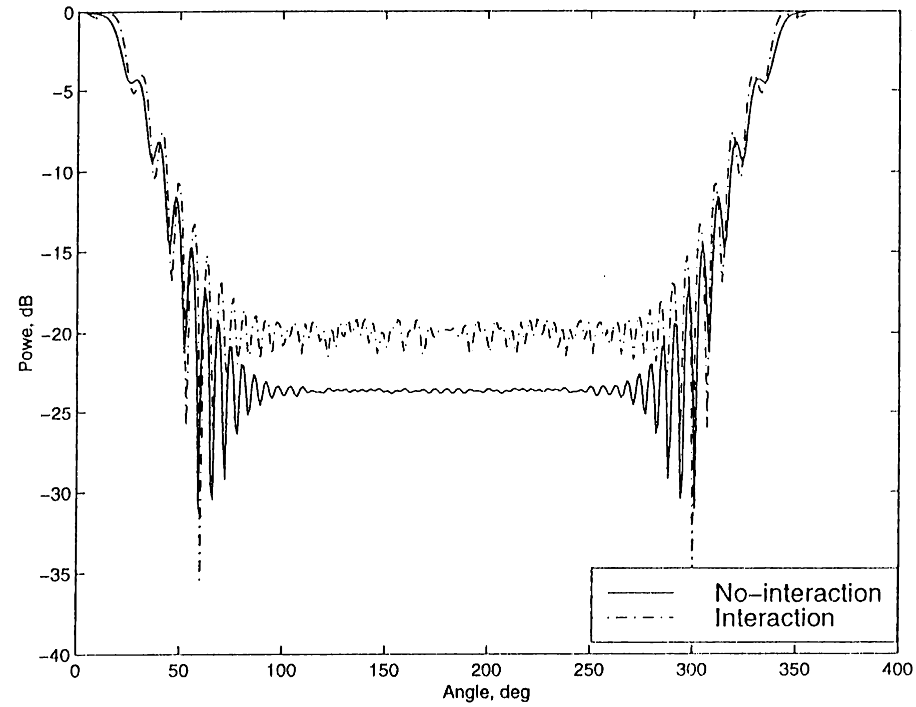

Figure 4.1: Power at far zone (for E polarization) for a grating consisting of four cylinders :M=4, kc=62.8, kb=5, beta=0, ka=0.4, N=5.

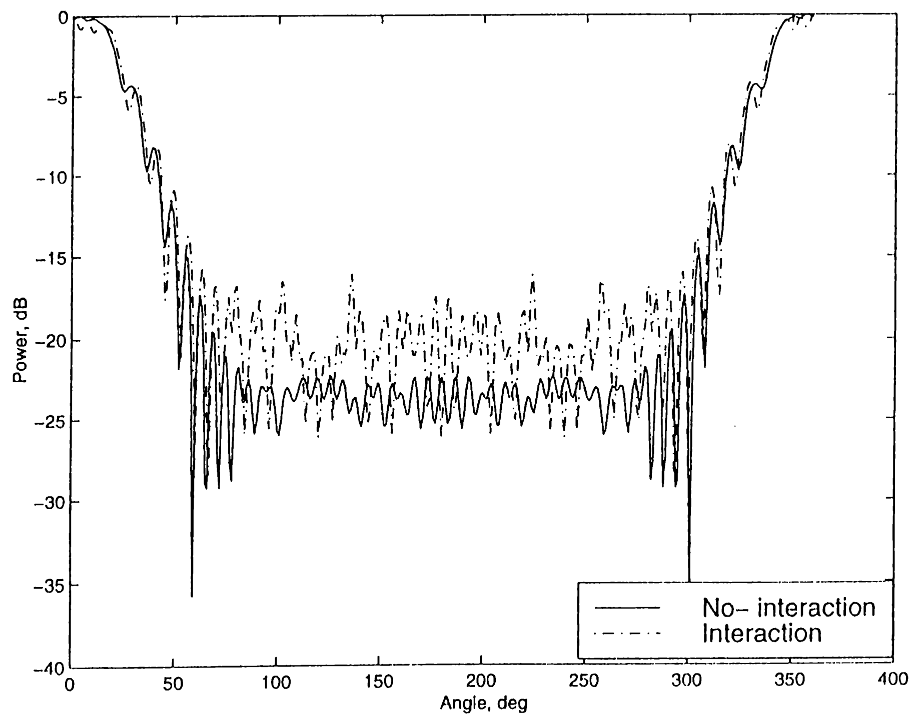

Figure 4.2: Power at far zone (for E polarization) for a grating consisting of six cylinders :M=6, kc=62.8, kb=5, beta=0, ka=0.4, N=5.

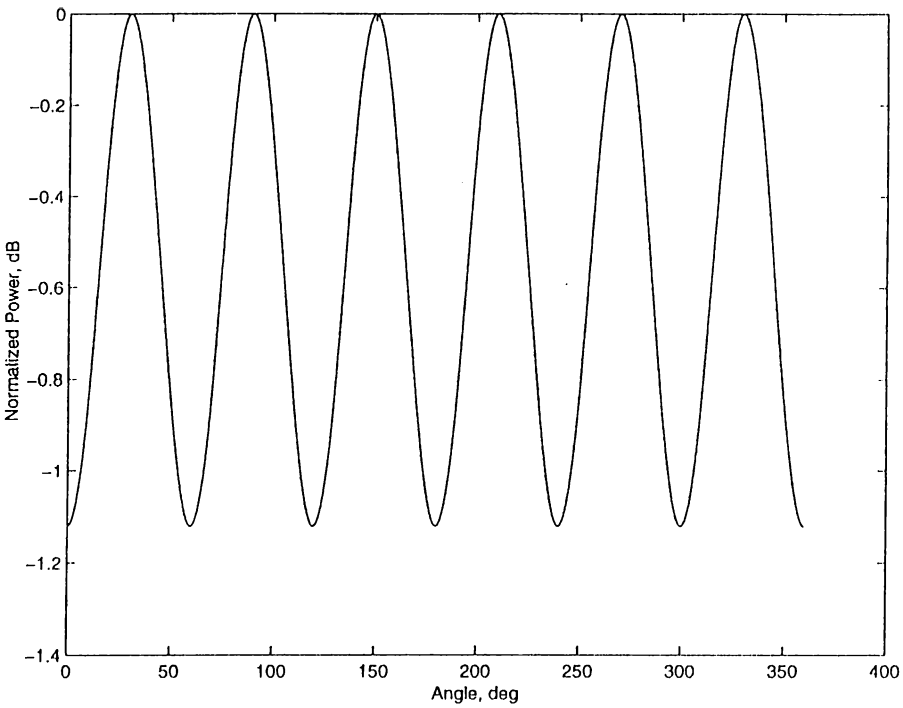

Figure 4.3: Power at far zone (for E polarization) for a grating consisting of six cylinders :M=6, ka=0.04, kc=3.14, N=4.

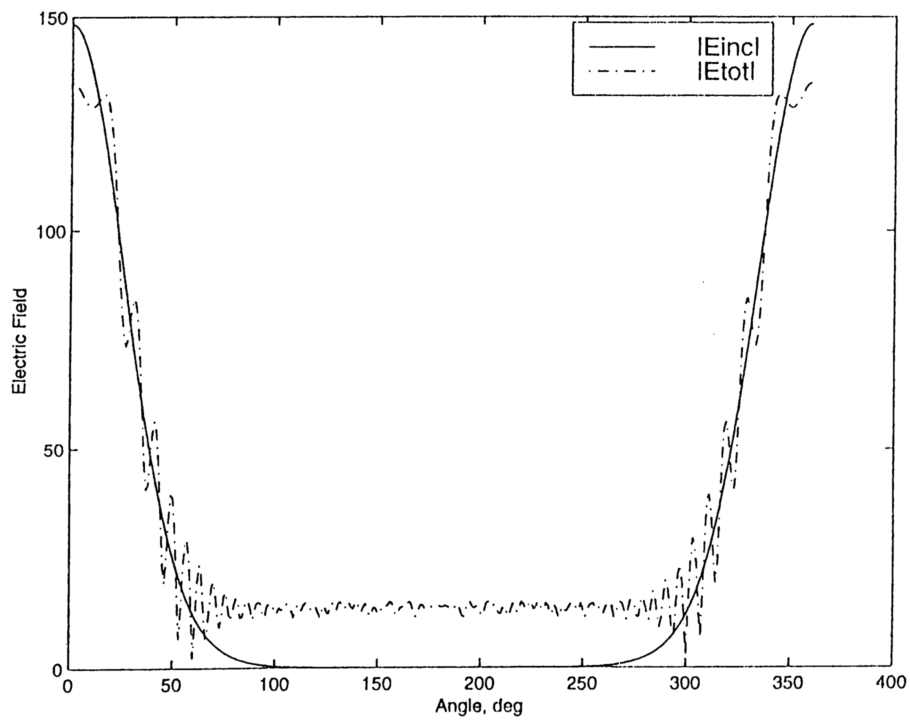

Figure 4.4: Electric field at far zone (for E polarization) for a grating consisting of two cylinders :M=2, kc=62.8, kb=5, beta=0, ka=0.4, N=5.

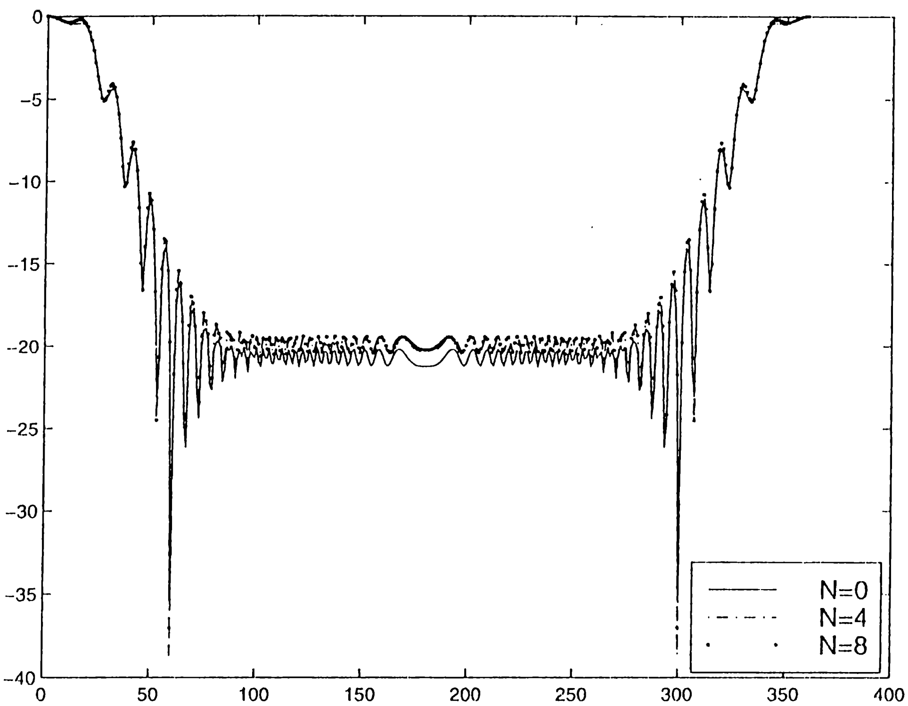

Figure 4.5: Power at far zone (for E polarization) for a grating consisting of two cylinders :M=2, ka=0.4, kb=5, kc=62.8, beta=0.

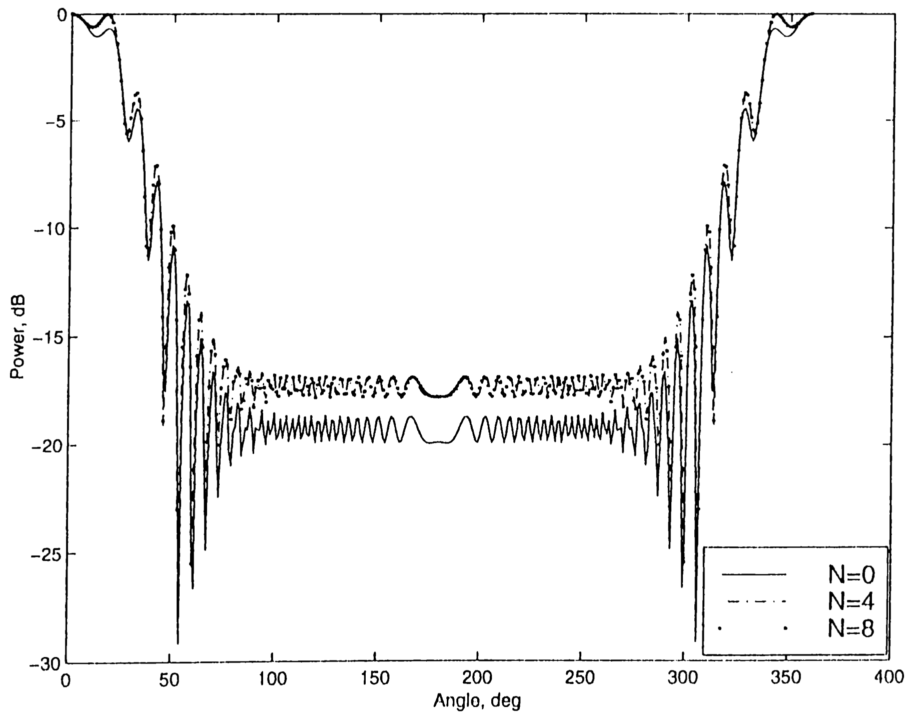

Figure 4.6: Power at far zone (for E polarization) for a grating consisting of two cylinders :M=2, ka=0.8, kb=5, kc=62.8, beta=0.

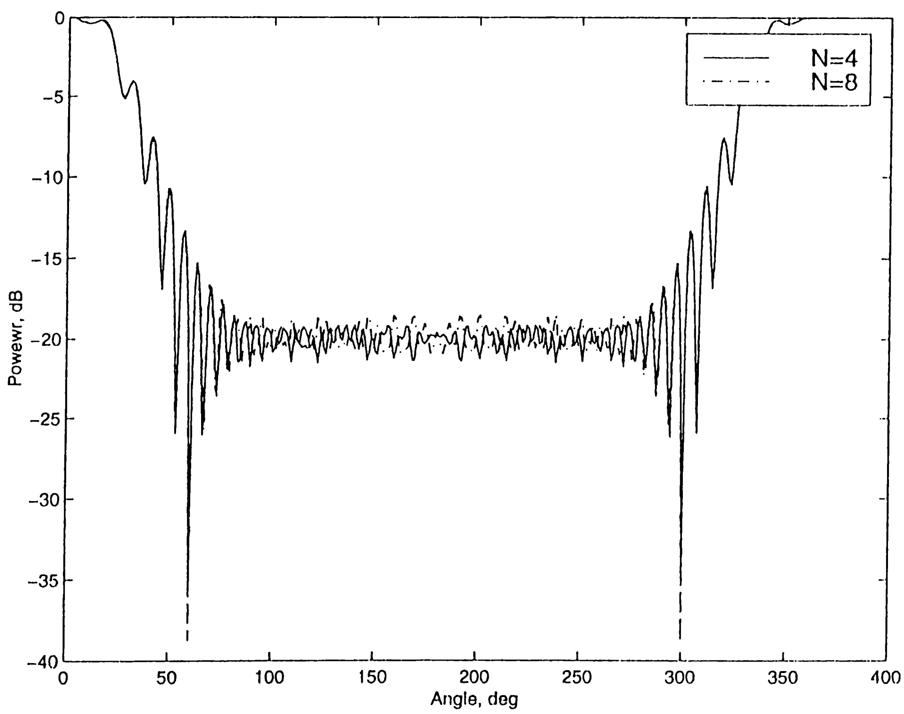

Figure 4.7: Power at far zone (for E polarization) for a grating consisting of four cylinders :M=4, ka=0.4, kb=5, kc=62.8, beta=0.

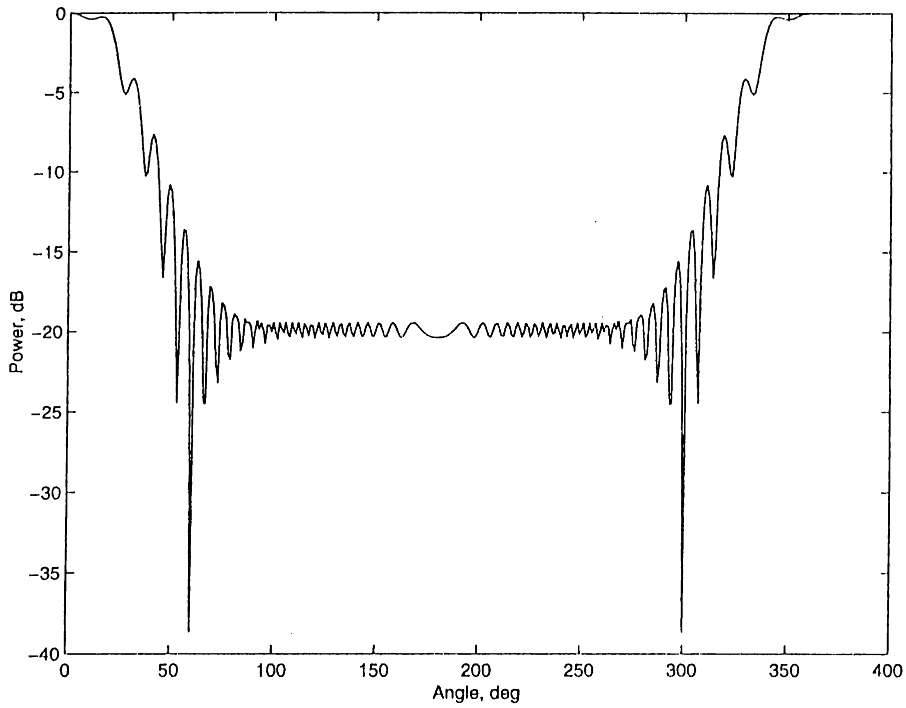

Figure 4.8: Power at far zone (for E polarization) for a grating consisting of two cylinders :M=2, ka=0.4, kb=5, kc=62.8, beta=0, N=5.

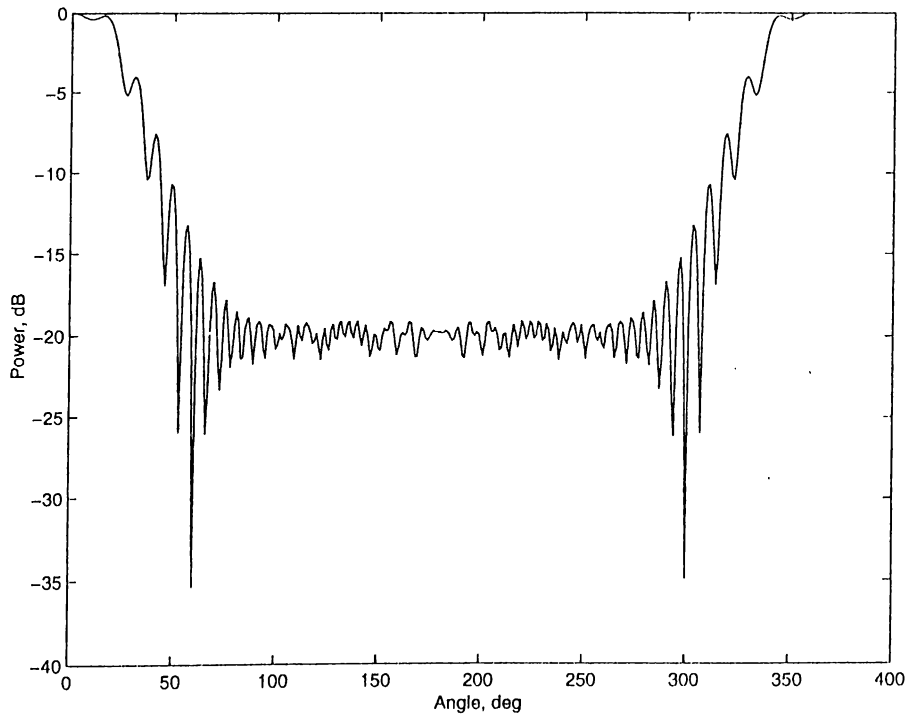

Figure 4.9: Power at far zone (for E polarization) for a grating consisting of four cylinders :M=4, ka=0.4, kb=5, kc=62.8, beta=0, N=5.

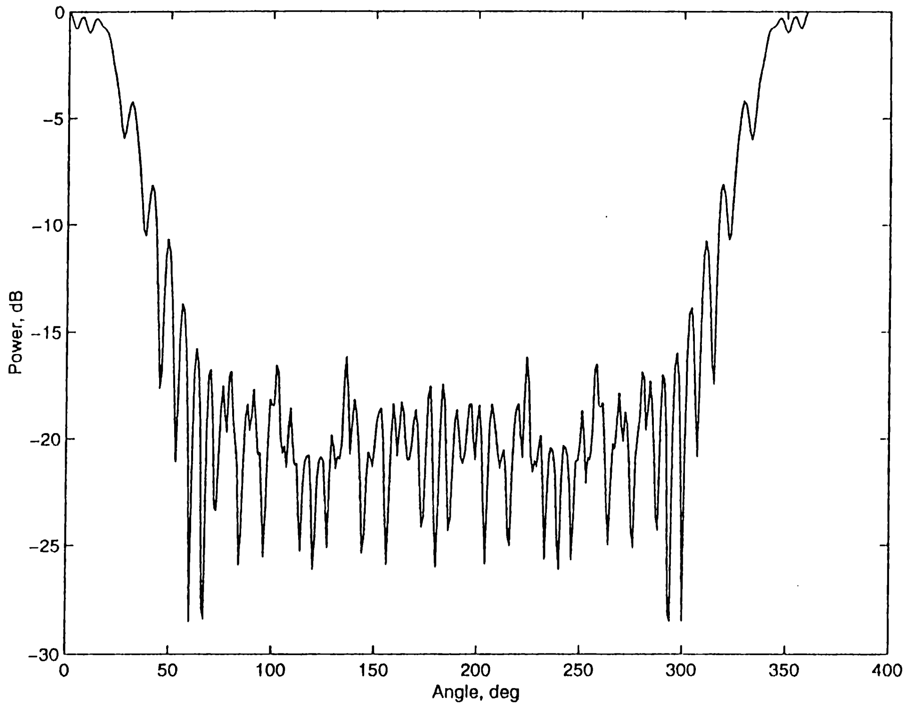

Figure 4.10: Power at far zone (for E polarization) for a grating consisting of six cylinders :M=6, ka=0.4, kb=5, kc=62.8, beta=0, N=5.

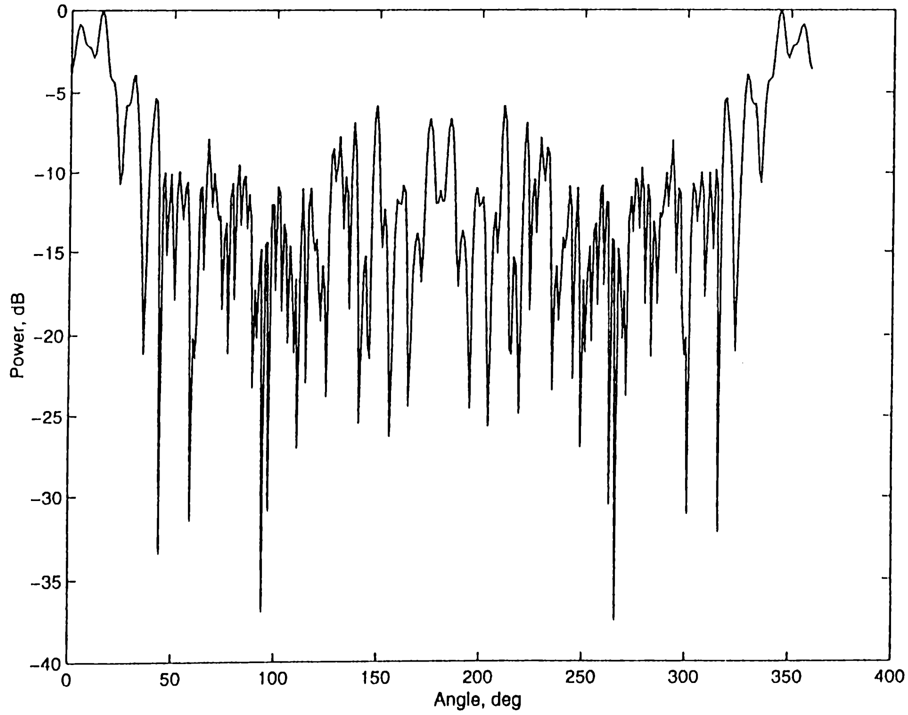

Figure 4.11: Power at far zone (for E polarization) for a grating consisting of ten cylinders :M=10, ka=0.4, kb=5, kc=62.8, beta=0, N=5.

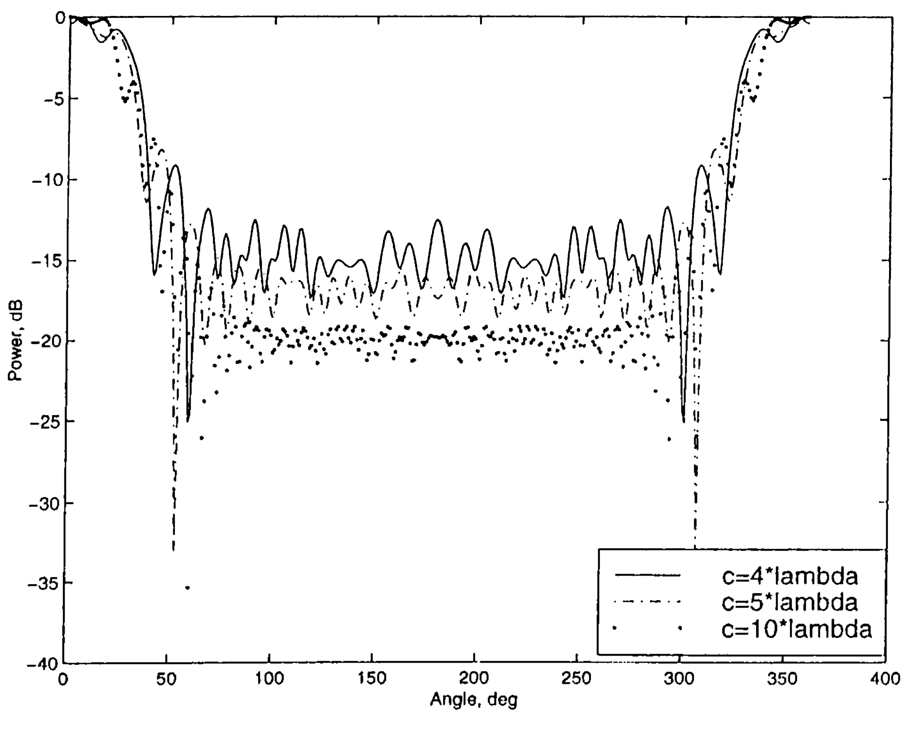

Figure 4.12: Power at far zone (for E polarization) for a grating consisting of four cylinders :M=4, kb=5,ka=0.4, beta=0, N=5.

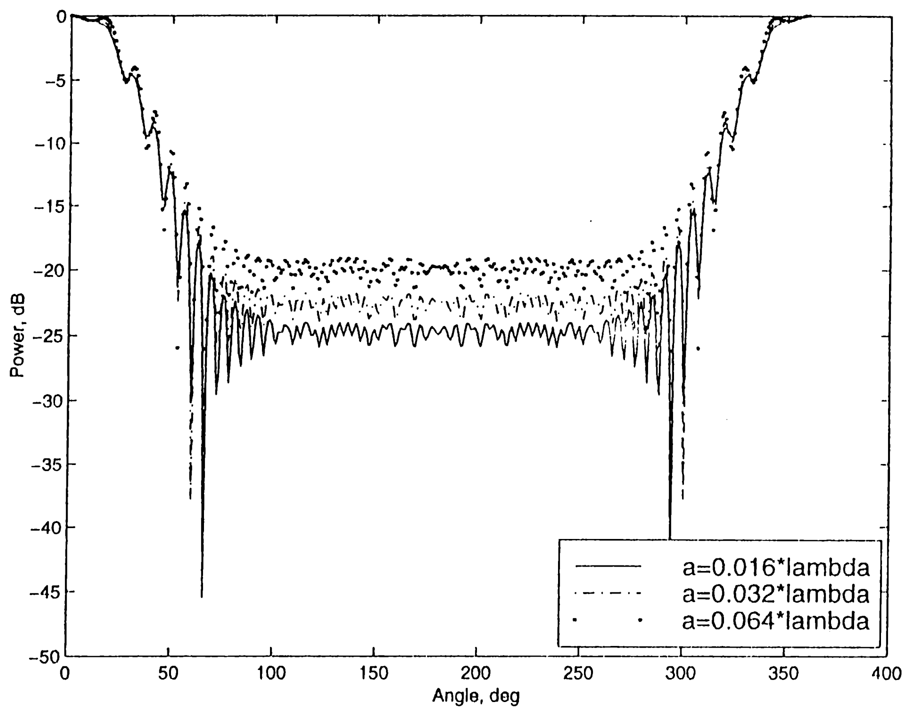

Figure 4.13: Power at far zone (for E polarization) for a grating consisting of four cylinders :M=4, kb=5, kc=62.8, beta=0, N=6.

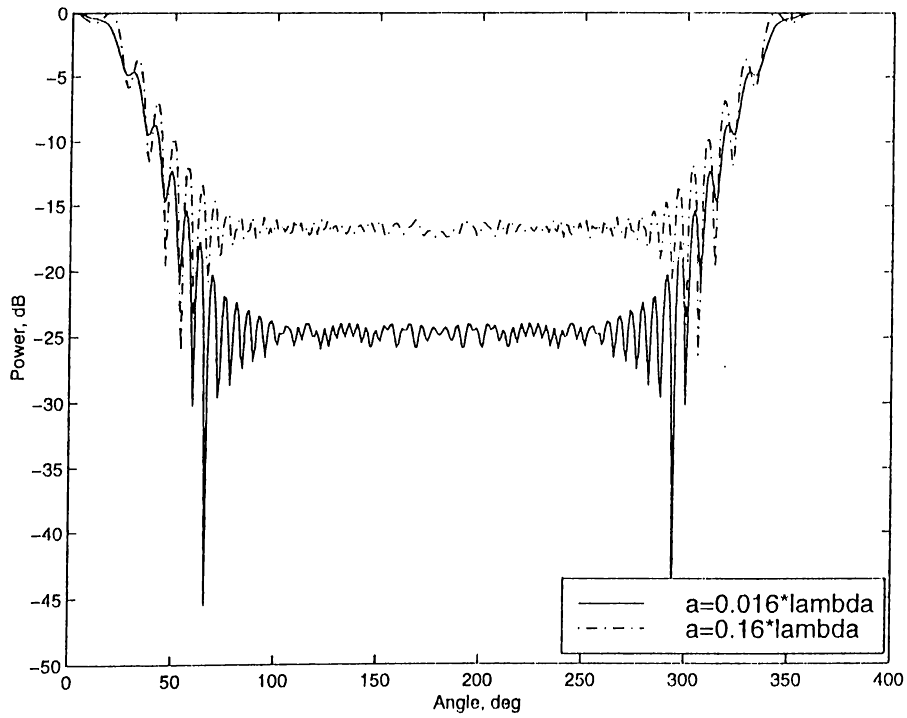

Figure 4.14: Power at far zone (for E polarization) for a grating consisting of four cylinders :M=4, kb=5, kc=62.8, beta=0, N=6.

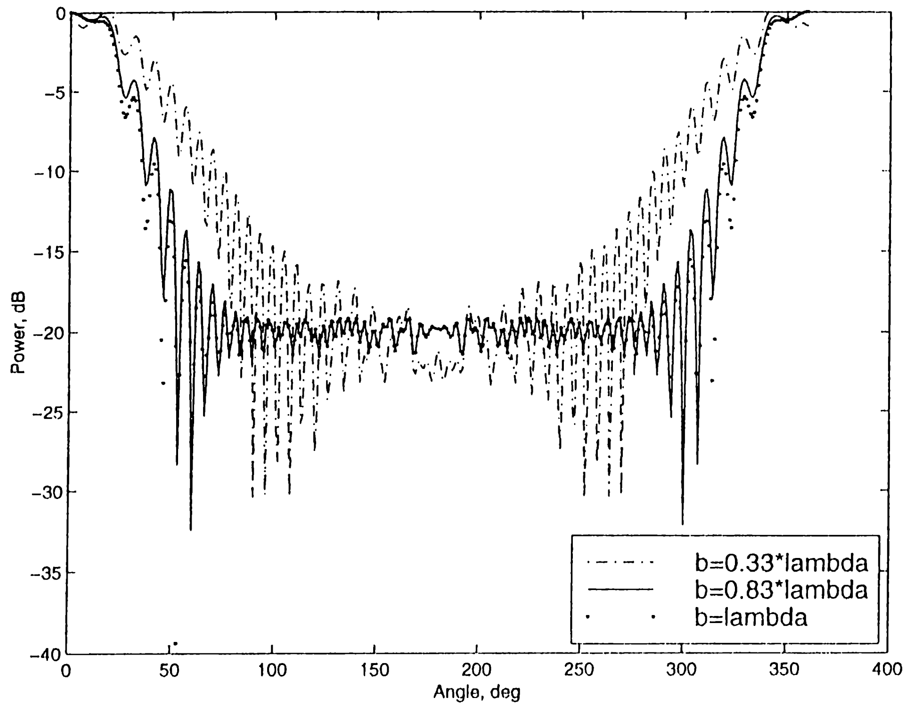

Figure 4.15: Power at far zone (for E polarization) for a grating consisting of four cylinders : ka=0.4, kc=62.8, beta=0, N=5

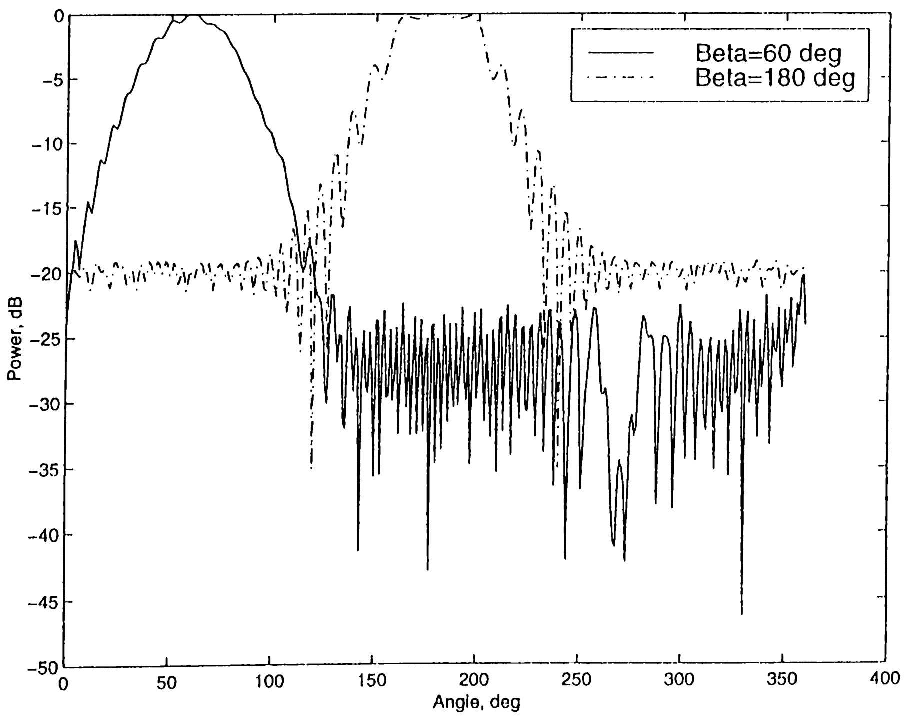

Figure 4.16: Power at far zone (for E polarization) for a grating consisting of four cylinders :M=4, ka=0.4, kb=5, kc=62.8, N=5.

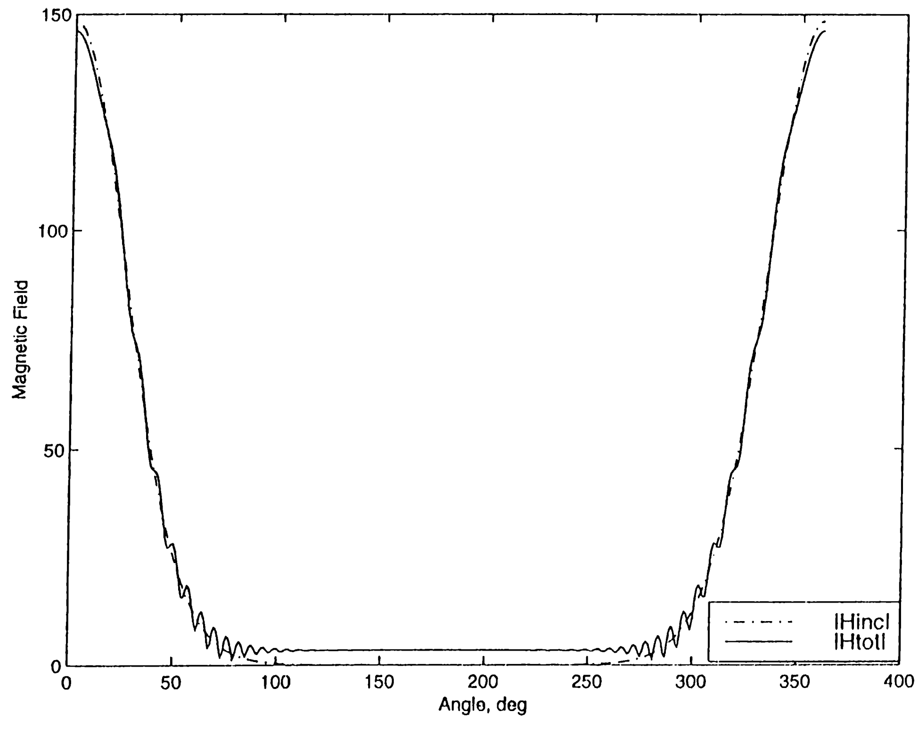

Figure 4.17: Magnetic Field (for H polarization) for free space and for two cylinders :ka=0.4, kb=5, kc=62.8, beta=0, N=5.

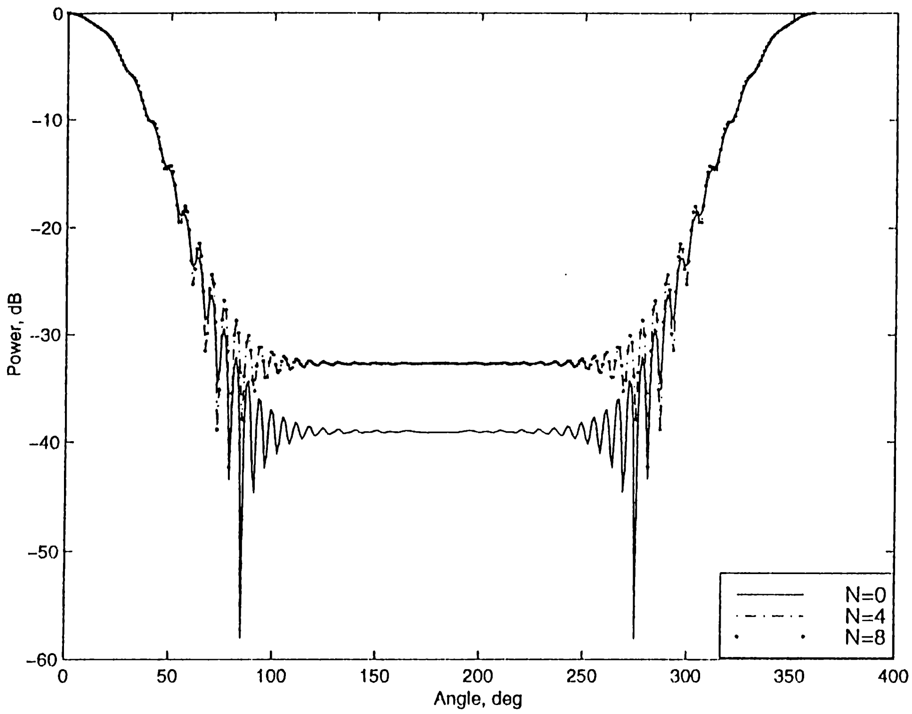

Figure 4.18: Power at far zone (for H polarization) for a grating consisting of two cylinders :M=2, ka=0.4, kb=5, kc=62.8, beta=0.

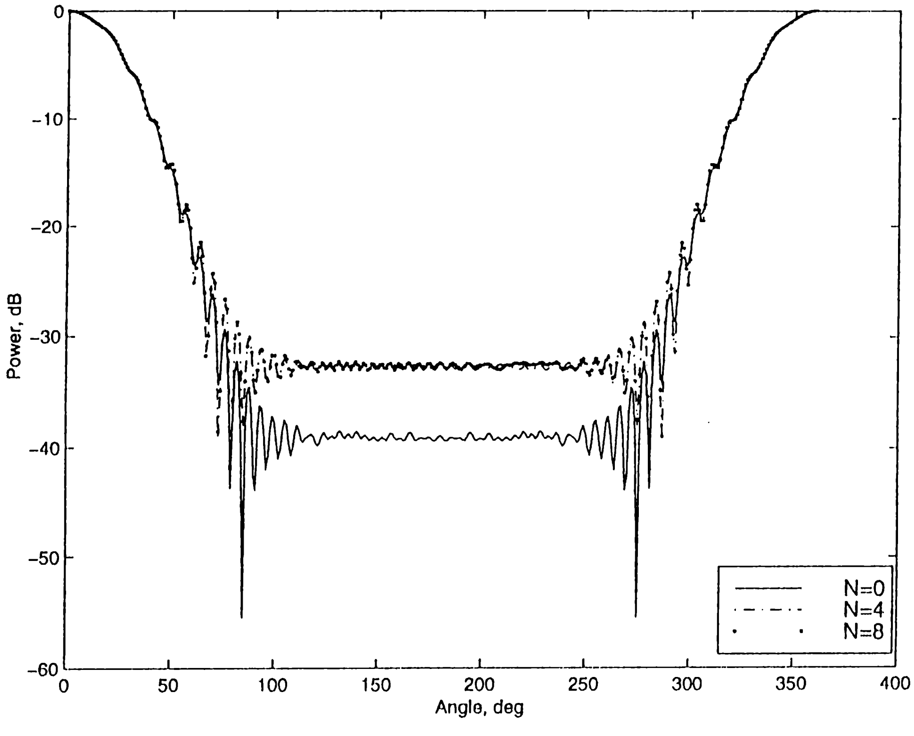

Figure 4.19: Power at far zone (for H polarization) for a grating consisting of four cylinders :M=4, ka=0.4, kb=5, kc=62.8, beta=0.

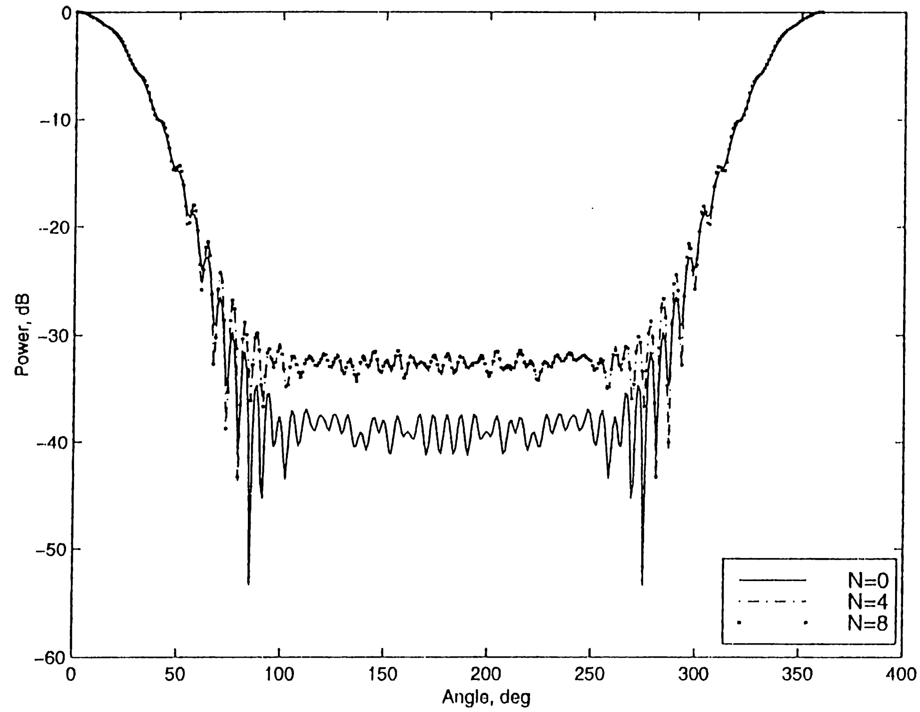

Figure 4.20: Power at far zone (for H polarization) for a grating consisting of six cylinders :M=6, ka=0.4, kb=5, kc=62.8, beta=0, N=4.

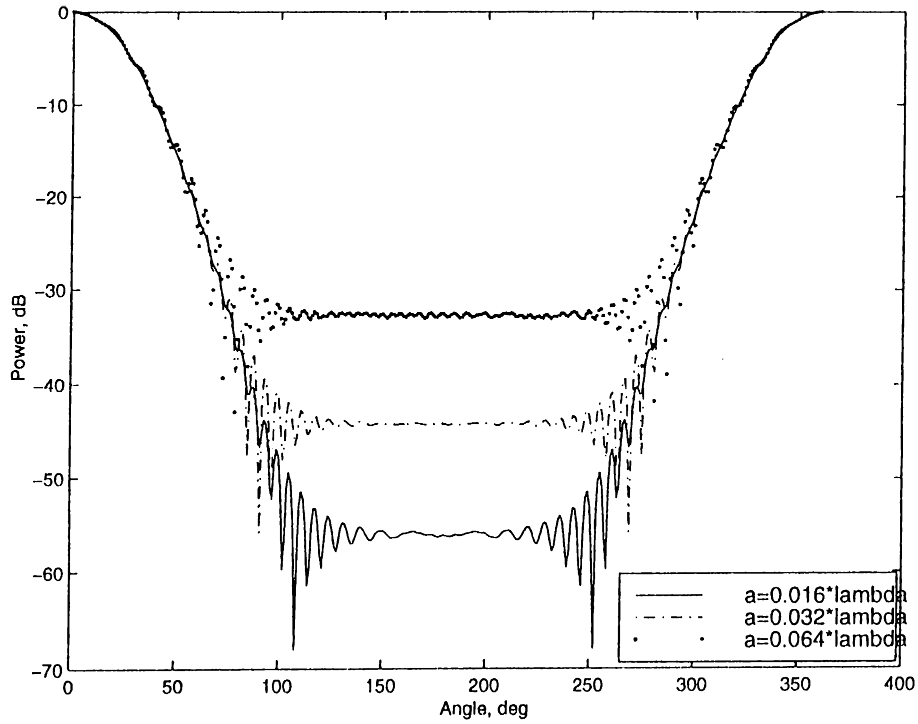

Figure 4.21: Power at far zone(for H polarization) for a grating consisting of four cylinders :M=4, kb=5, kc=62.8, beta=0, N=5.

4.2 Directivity

One very important description of an antenna is how much it concentrates energy in one direction in preference to radiation in other direction. This characteristics of an antenna is called directivity.

Directivity is the ratio of the maximum radiation intensity to the average radiation intensity,

$$D = \frac{U_{max}}{U_0} \tag{4.3}$$

where U is the radiation intensity(w/unit solid angle)

$$U = \frac{r^2}{2\eta}|E|^2 \tag{4.4}$$

and η is the intrinsic impedance. The formula of the directivity in terms of electric field intensity is as follows

$$D = \frac{2\pi |E^{max}|^2}{\int_0^{(2\pi)} |E(\phi)|^2 d\phi}. \tag{4.5}$$

In order to avoid the integral, we use Parseval's Relation:

$$\frac{1}{T_o}\int_{T_o} |x(t)|^2 dt = \sum_n |a_n|^2 \tag{4.6}$$

where a_n are the angular Fourier expansion coefficients of the field in far- zone. We can write the formula for directivity in E polarization by using Parseval's Relation as

$$D = \frac{|E^{max}|^2}{\sum_n |a_n|^2}. \tag{4.7}$$

In this study, for E-polarization a_n have been found as

$$a_n = j^n J_n(k_0 r_s) e^{-jn\phi_s} + j^{2n} J_n(k_0) c \sum_{m=1}^{M} C_{mn} e^{-jn\phi_m}. \tag{4.8}$$

For H-polarization a_n is given as

$$a_n = j^n J_n(k_0 r_s) e^{-jn\phi_s} + j^{2n} J_n(k_0) c \sum_{m=1}^{M} D_{mn} e^{-jn\phi_m}, \tag{4.9}$$

where $r_s = jb$, b is related to the beam width, $\phi_s = \beta$, β is the beam direction, ϕ_m is the angle between the observation direction and mth cylinder. Directivity of the source is analyzed for both E and H polarization.

4.2.1 E Polarization

In order to show how the directivity of the source is effected by the grating structure and its parameters, the Figures 4.22 through 4.29 are plotted. If we look at the Figure 4.22, the directivity of the source in free space does not change with beam direction. It does not depend on the beam direction. If the source is near a single cylinder, the directivity changes with beam direction. When the beam is directed toward the cylinder, the minimum directivity is obtained. When the beam is declined by about 18^0 from the nearest cylinder, the maximum directivity is obtained. Because, when the beam is directed toward the cylinder, the conducting cylinder scatters the field at backward direction and at this point the interference of incident field and scattered field is destructive and the maximum field decreases. Thus, directivity is decreased. On the other hand, when the beam is declined by about 18^0 from the nearest cylinder, the field is scattered in all directions. The superposition of the incident field and the scattered field occurs, and the interference appears to be constructive. Thus, the maximum amplitude of the total field is obtained.

In Figures 4.23 through 4.27, the directivity of the source for gratings consisting of a periodic array of two, three, four, five and six conducting cylinders is obtained. In these figures, the directivity variations versus the beam direction are presented. The variations of directivity with beam direction is effected by the number of cylinders. When we increase number of cylinders on the surface of the grating, the oscillation of the directivity between two cylinders decreases. The maximum directivity is obtained when the beam is declined about 18^0 from the nearest cylinder.

Figures 4.27 and 4.28 present how the directivity changes with changing cylinder radius for various numbers of cylinders on the surface of the grating. As expected, increasing the radius a decreases the directivity. Number of cylinders do not affect the dependence of the overall directivity versus cylinder radius very much.

The directivity variations versus grating radius c are presented in Figure 4.29 for grating of two cylinders when $k_0a = 0.4$, $k_0b = 5$, $\beta = 0$, $r_0 = 0$ and $N = 5$. From this figure, we can see that, when we increase grating radius, the directivity makes oscillations with decreasing magnitude as a function of the grating radius. It is caused by the in-phase or out-phase superposition of the incident and scattered fields which depends on the distance between the source and the cylinder. The period of this oscillation is about $\lambda/4$. Since the effect of the dielectric radome is optimized when $2c = n\lambda/2$. Thus, $c = n\lambda/4$

for $n = 1, 2, ...$

The relation between directivity and frequency of the source is presented in Figures 4.30, 4.31 and 4.32. Figure 4.33 shows how directivity depends on wavelength. In these figures, directivity makes oscillations with frequency and wavelength. The reason of this is related to the effect explained in the preceding paragraph since the frequency and wavelength of the source is directly related to the wave number (k_0). The wave number affect the phase of the fields.

4.2.2 H Polarization

The directivity of the source for grating consisting of a periodic array of one, two, four, six cylinders are presented in Figures 4.34 through 4.37. The variations of directivity with beam direction is effected by the number of cylinders. The directivity versus beam direction in H polarization is similar to the directivity versus beam direction in E polarization. The differences between them are related to the magnitude of the directivity and changing when beam direction is near the cylinder. In H polarization because of the edge diffraction, the minimum directivity is obtained when the beam is declined by about 10^0 from the nearest cylinder and the maximum directivity is obtained when the beam is declined by about 20^0 from the nearest cylinder. The amplitude of the oscillation is less the mplitude of the oscillation in E polarization.

The directivity variations versus grating radius c are presented in Figure 4.38 for grating of two cylinders when $k_0a = 0.4$, $k_0b = 5$, $\beta = 0$, $r_0 = 0$ and $N = 5$. From this figure, we can see that, when we increase the grating radius, the directivity makes oscillations with decreasing magnitude as a function of the radome radius. It is caused by the in-phase or out of phase which depend on the distance between source and cylinder interference of the incident field and scattered field. The period of this oscillation is about $\lambda/4$.

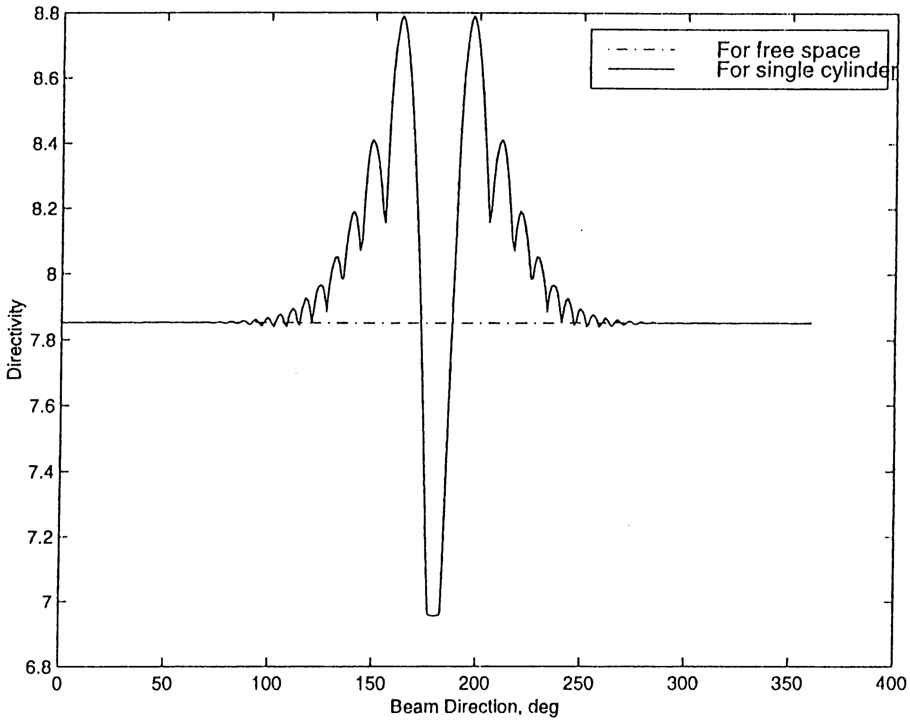

Figure 4.22: Directivity versus Beam Direction (for E polarization) for a grating consisting of single cylinder:kc=62.8, kb=5; ka=0.4, N=5.

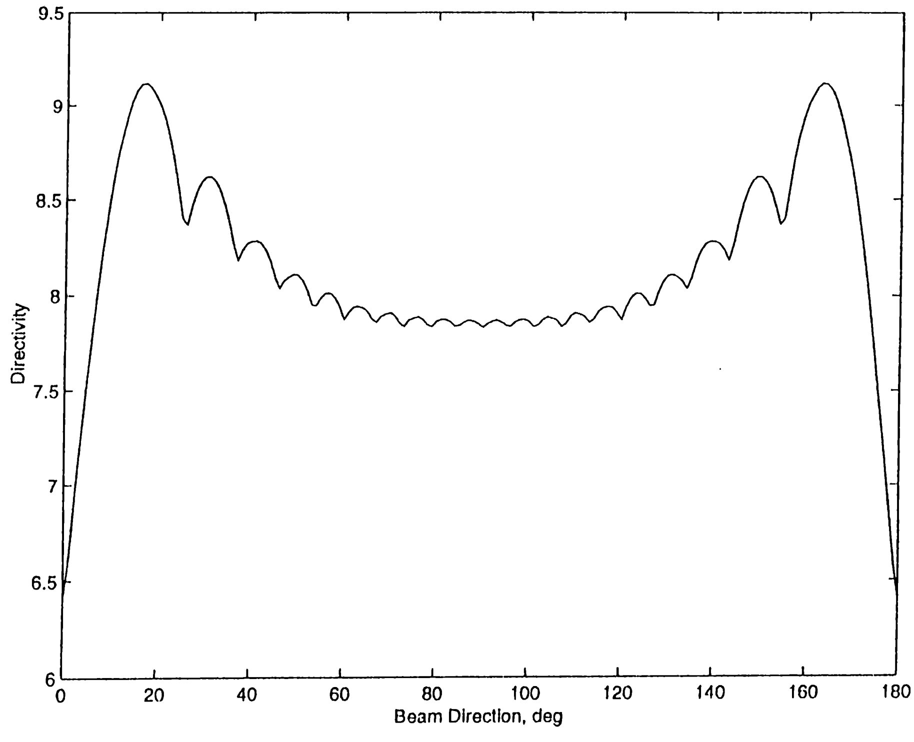

Figure 4.23: Directivity versus Beam Direction (for E polarization) for a grating consisting of two cylinders:M=2, kc=62.8, kb=5;ka=0.4, N=5.

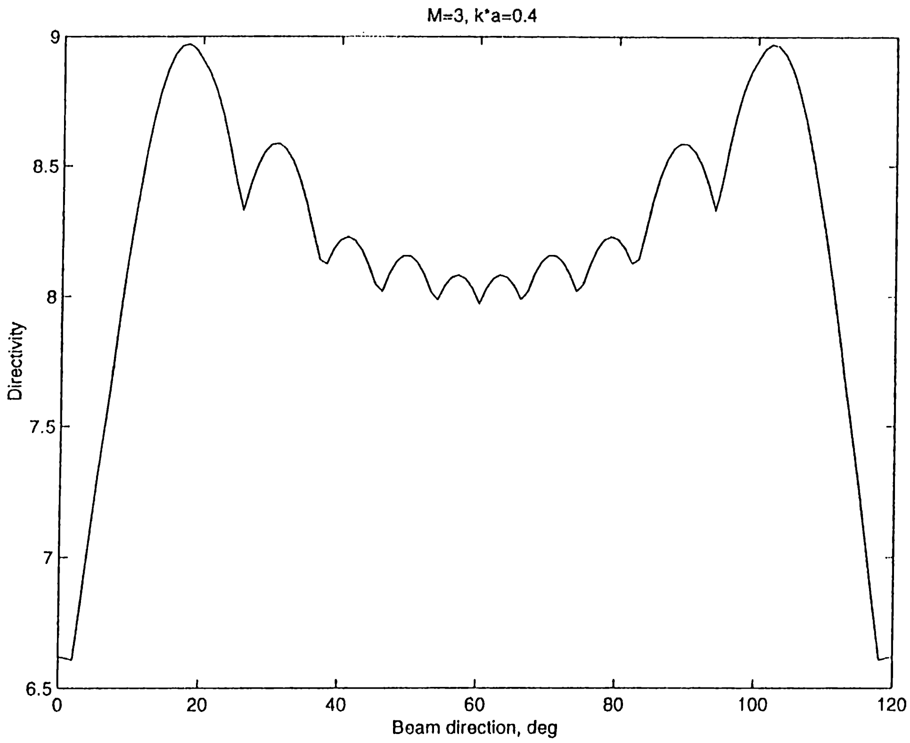

Figure 4.24: Directivity versus Beam Direction (for E polarization) for a grating consisting of three cylinders:M=3, kc=62.8, kb=5, ka=0.4, N=5.

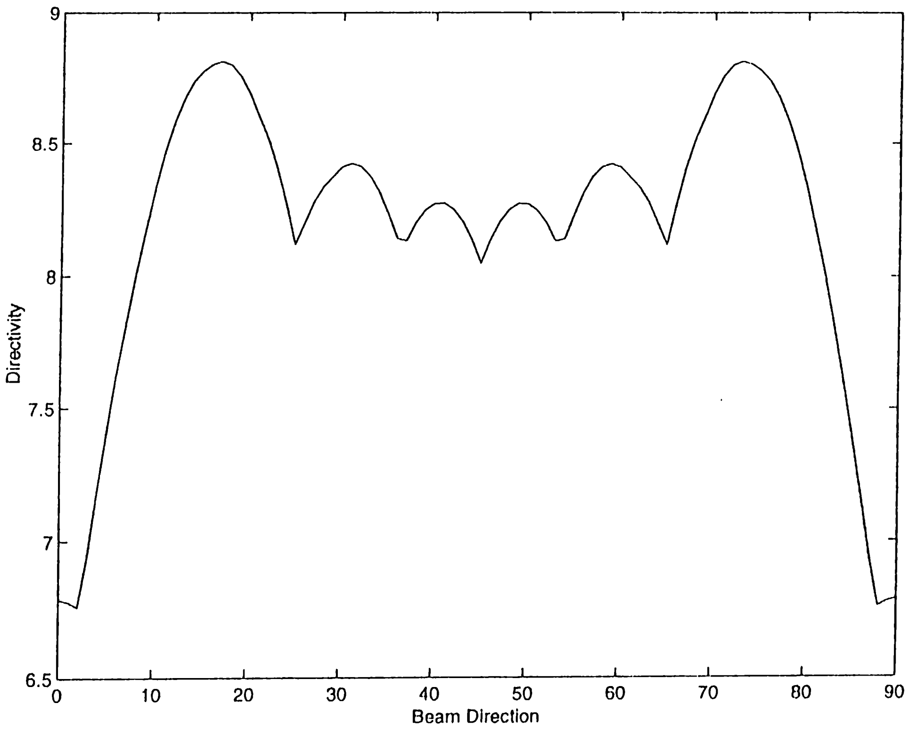

Figure 4.25: Directivity versus Beam Direction (for E polarization) for a grating consisting of four cylinders:M=4, kc=62.8, kb=5, ka=0.4, N=5.

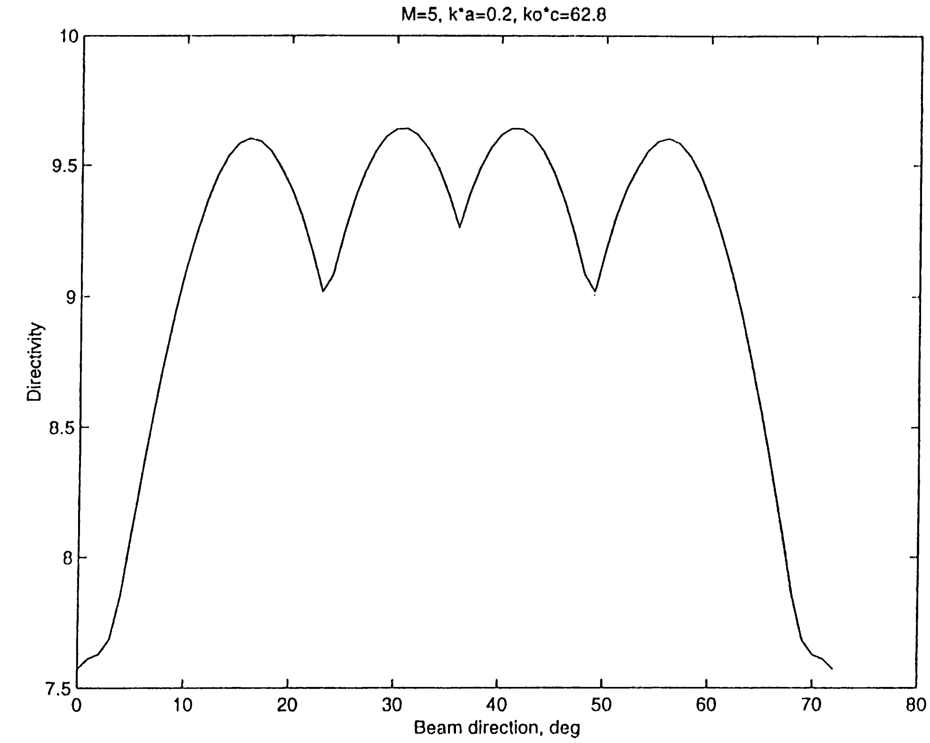

Figure 4.26: Directivity versus Beam Direction (for E polarization) for a grating consisting of five cylinders:M=5, kc=62.8, kb=5; ka=0.2, N=4.

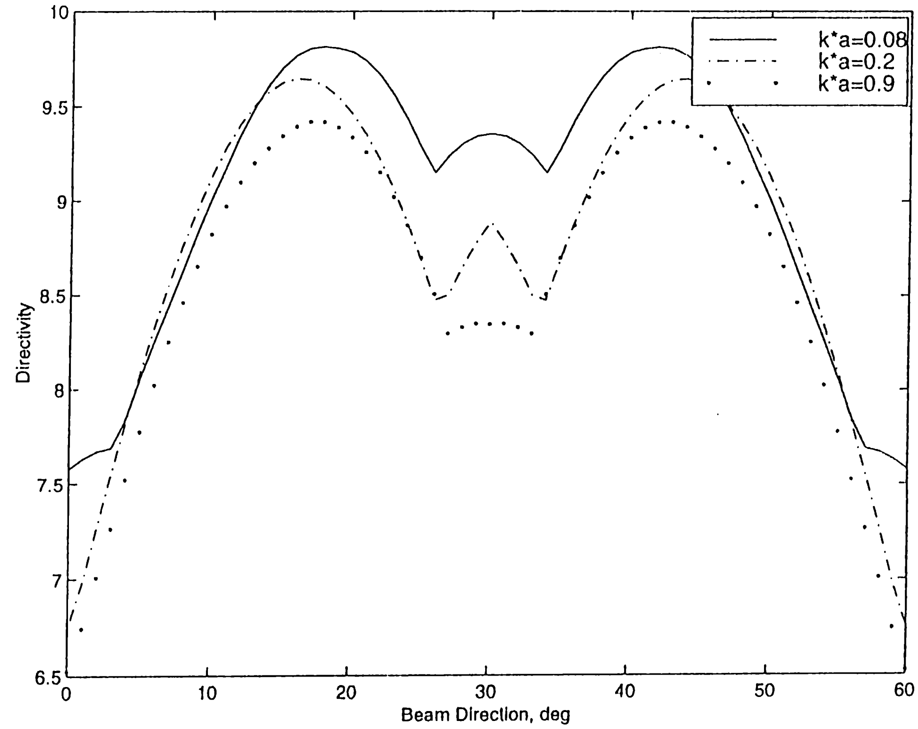

Figure 4.27: Directivity versus Beam Direction (for E polarization) for a grating consisting of six cylinders:M=6, kc=62.8, kb=5, N=6.

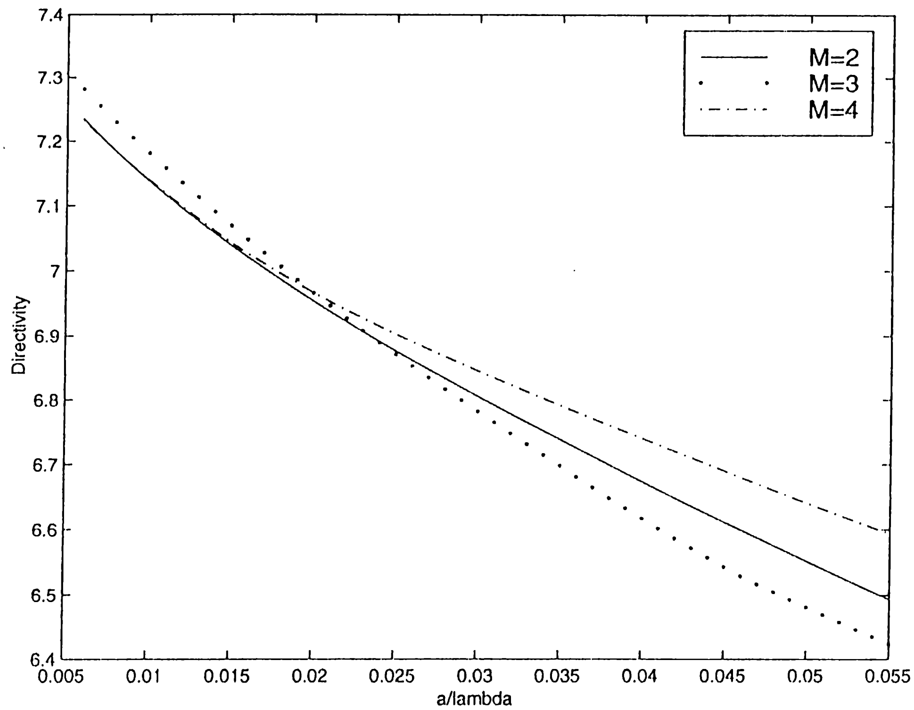

Figure 4.28: Directivity versus radius of cylinders (for E polarization) :kc=62.8, kb=5, beta=0, N=5.

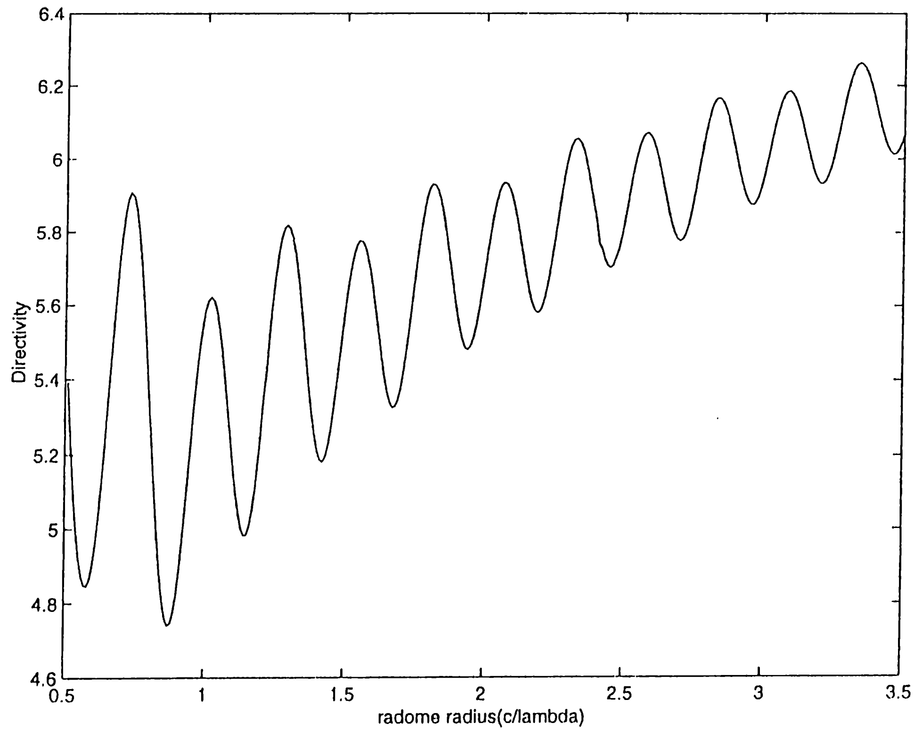

Figure 4.29: Directivity versus grating radius (c) (for E polarization) for a grating consisting of two cylinders: M=2, ka=0.4, kb=5, beta=0, N=4.

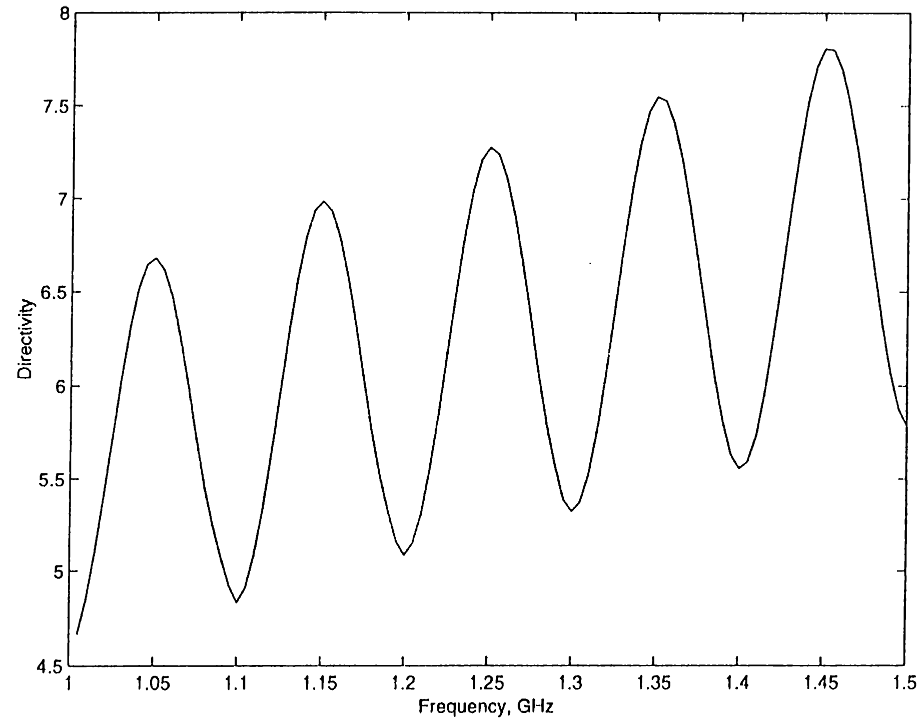

Figure 4.30: Directivity versus frequency (for E polarization) for a grating consisting of two cylinders :M=2, c=1.5m, a=1cm, b=12cm, beta=0, N=5.

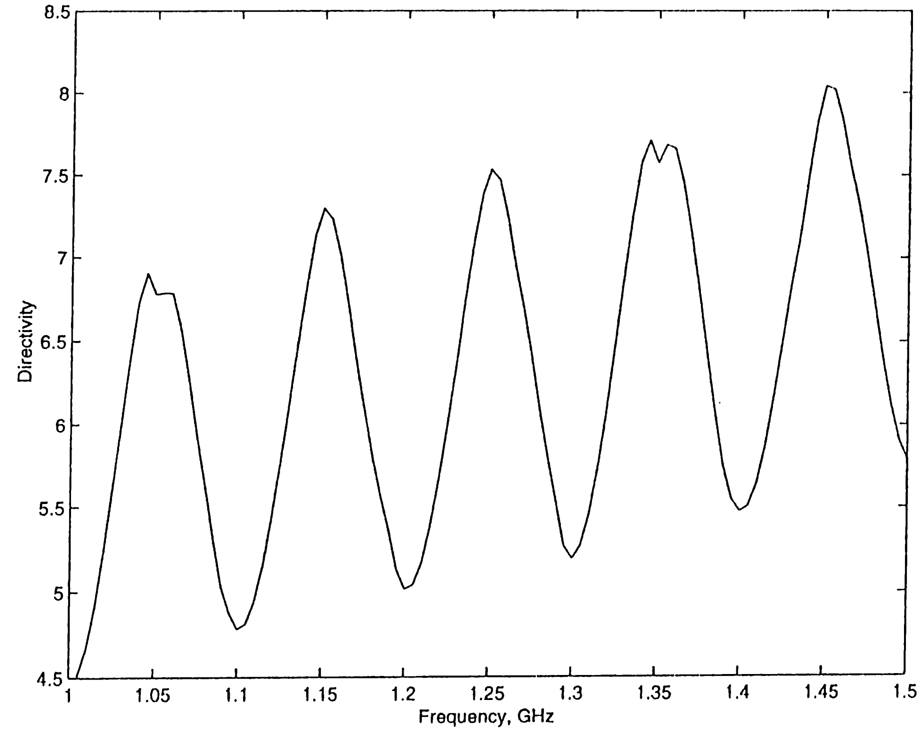

Figure 4.31: Directivity versus frequency (for E polarization) for a grating consisting of four cylinders :M=4, c=1.5m, a=1cm, b=12cm, beta=0, N=5.

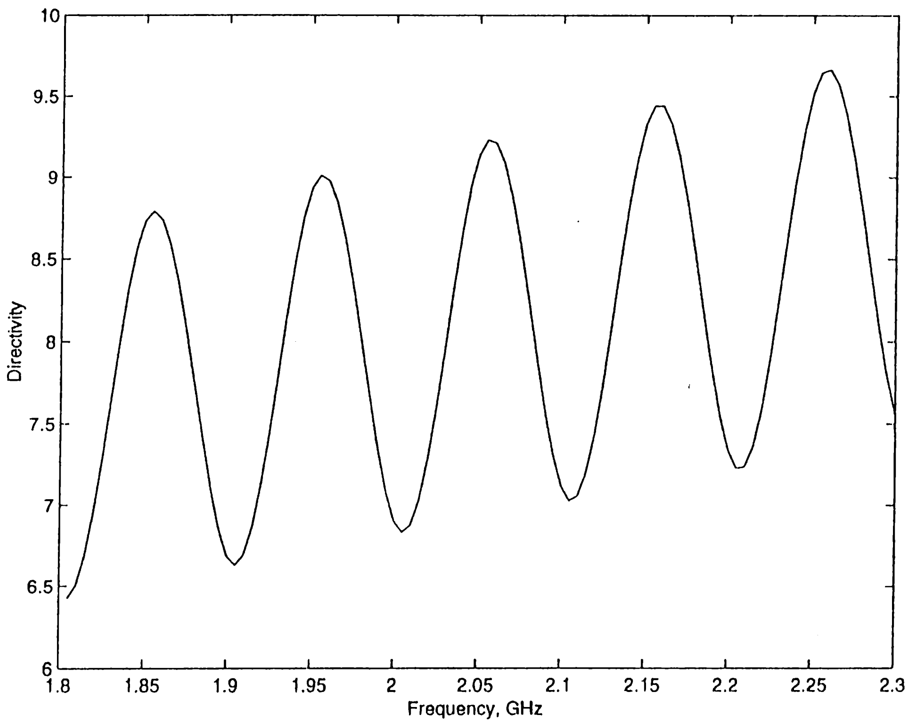

Figure 4.32: Directivity versus frequency (for E polarization) for a grating consisting of two cylinders :M=2, c=1.5m, a=1cm, b=12cm, beta=0, N=5.

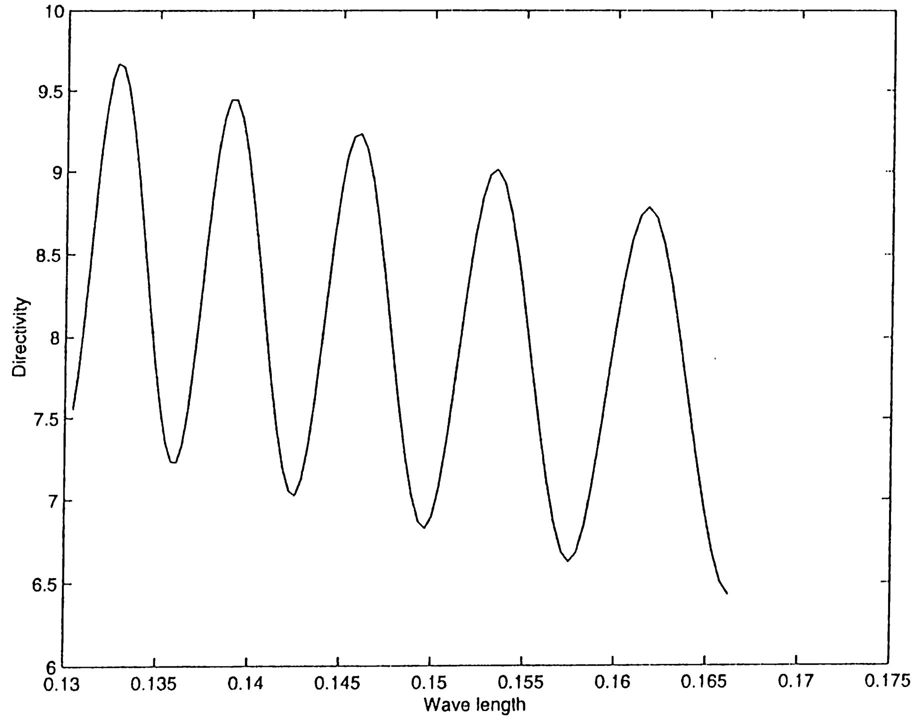

Figure 4.33: Directivity versus wave length (for E polarization) for a grating consisting of two cylinders :M=2, c=1.5m, a=1cm, b=12cm, beta=0, N=5.

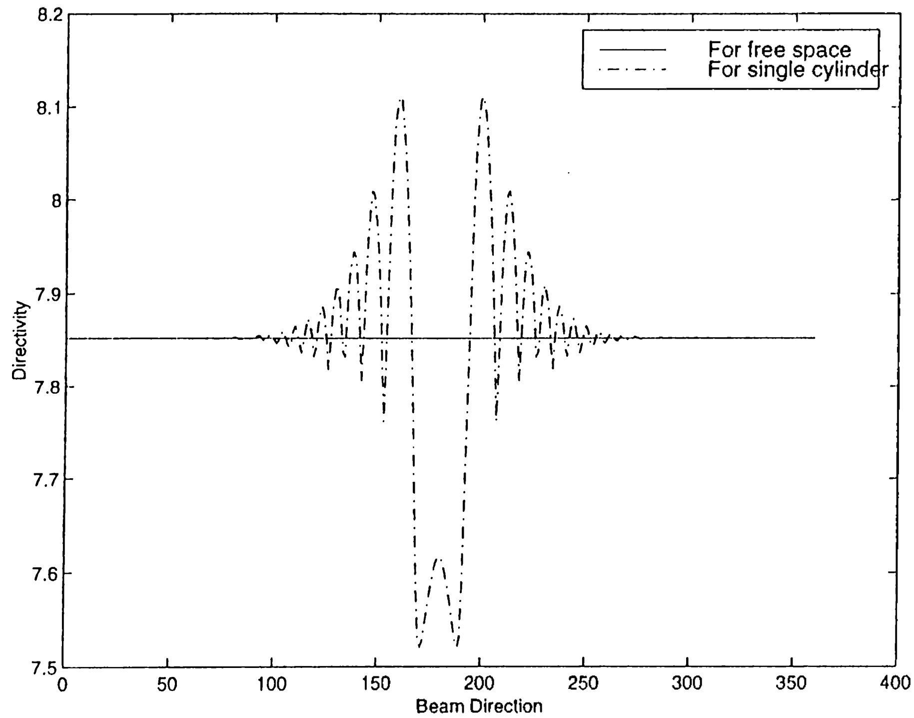

Figure 4.34: Directivity versus Beam Direction (for H polarization) for a grating consisting of a single cylinder: kc=62.8, kb=5, ka=0.4, N=5.

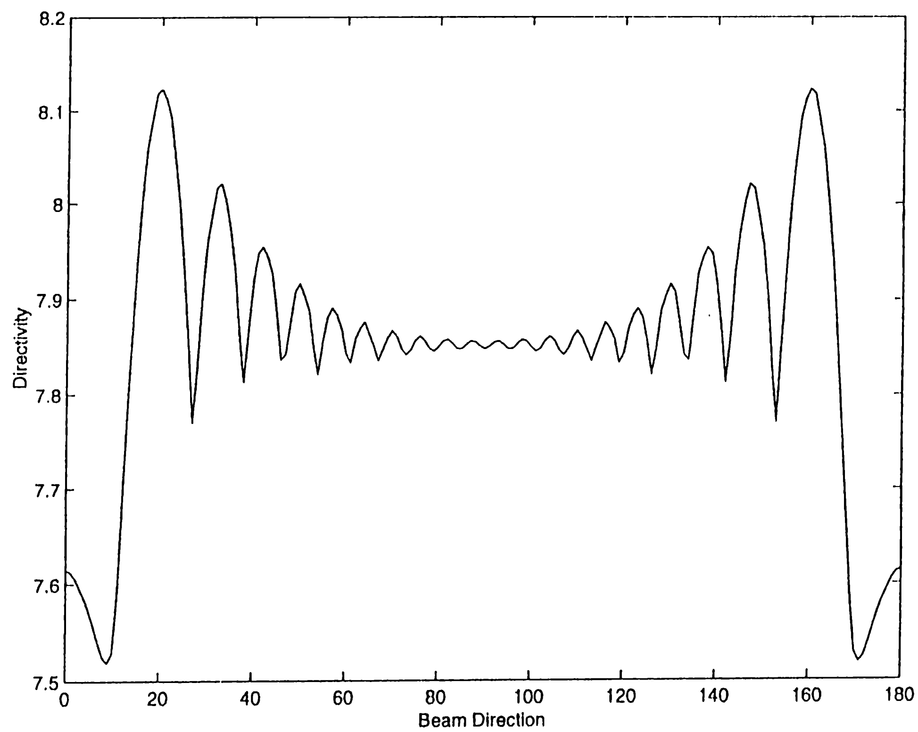

Figure 4.35: Directivity versus Beam Direction (for H polarization) for a grating consisting of two cylinders:M=2, kc=62.8, kb=5, ka=0.4, N=5.

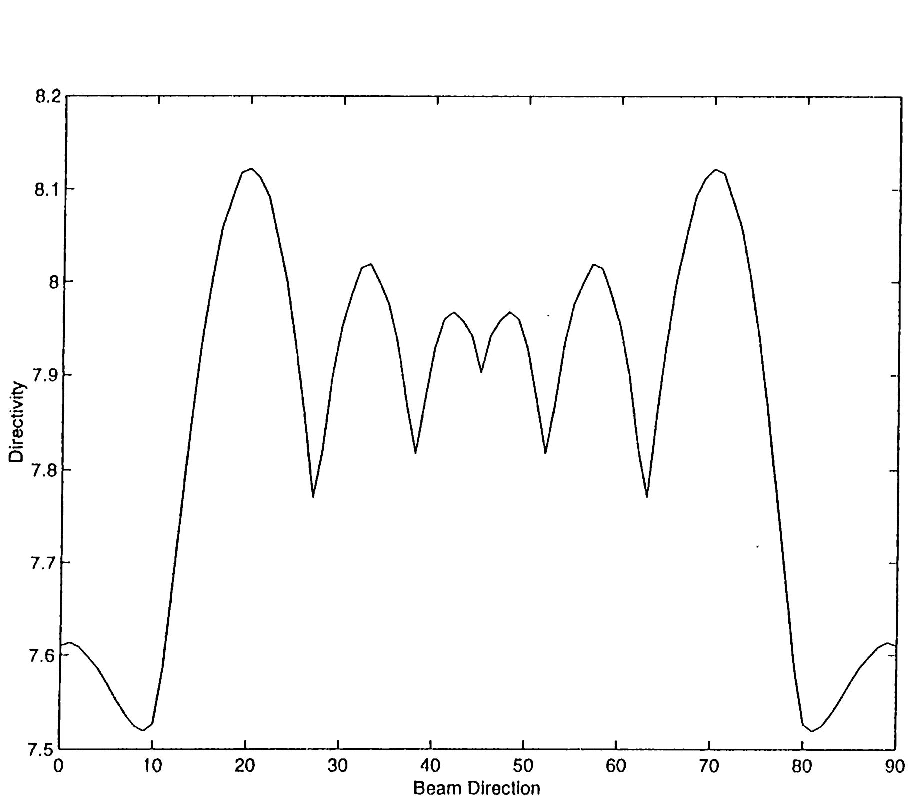

Figure 4.36: Directivity versus Beam Direction (for H polarization) for a grating consisting of four cylinders:M=4, kc=62.8, kb=5, ka=0.4, N=5.

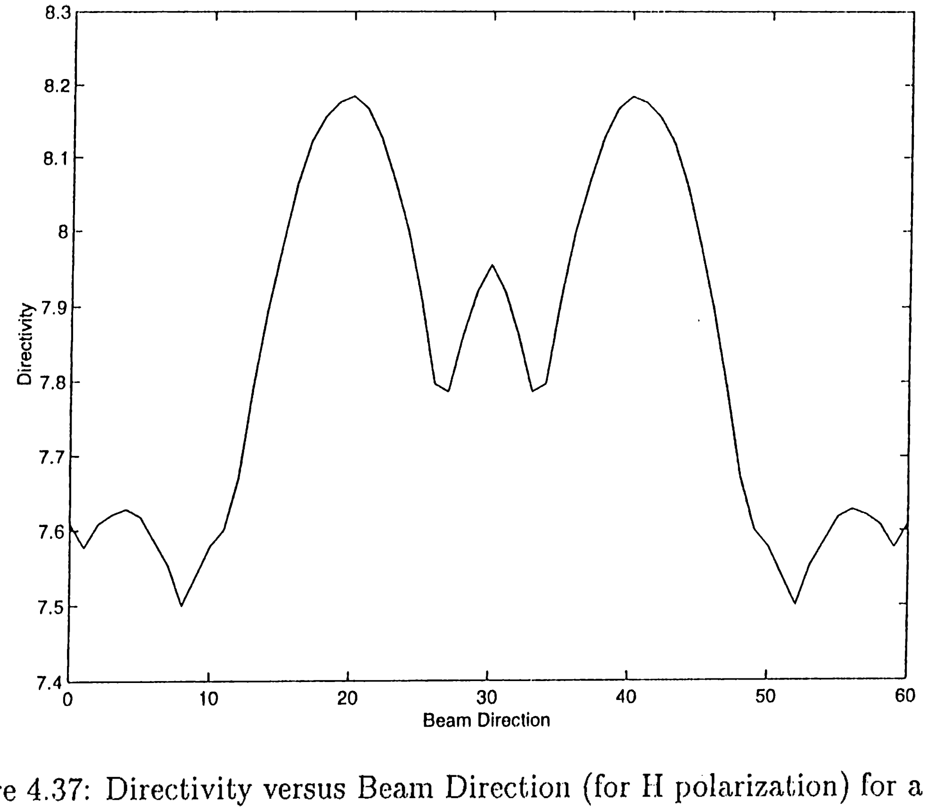

Figure 4.37: Directivity versus Beam Direction (for H polarization) for a grating consisting of six cylinders:M=6, kc=62.8, kb=5, ka=0.4, N=5.

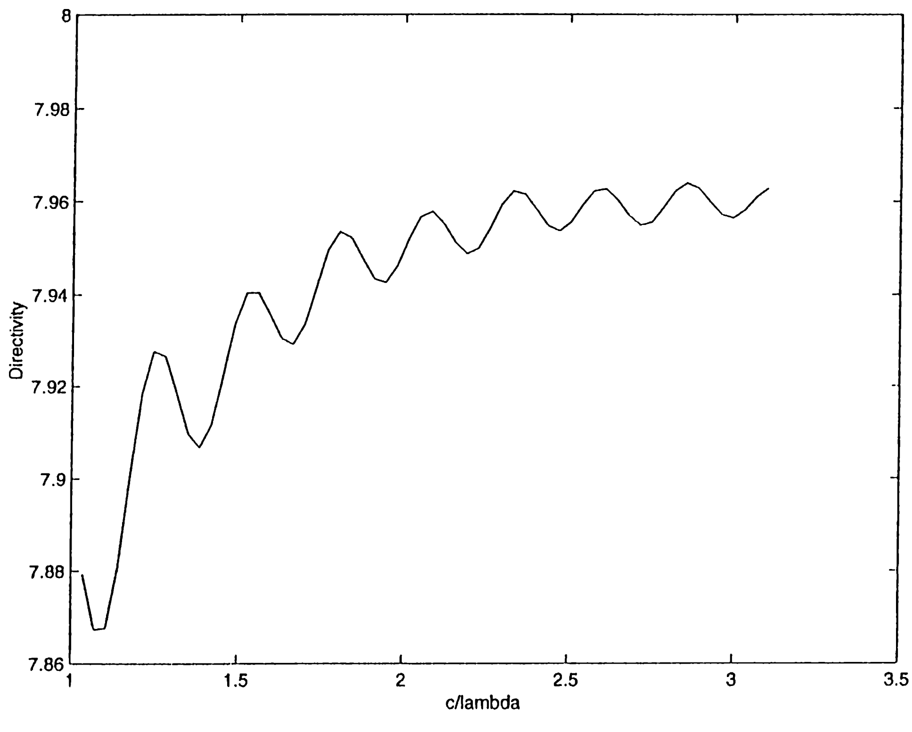

Figure 4.38: Directivity versus radome radius (for H polarization) for a grating consisting of two cylinders:M=2, kb=5, ka=0.4, N=5.

4.3 Complex Source Position

We have two cases for complex source position: one is the source at the center of the structure, the other case is the source shifted from the center of the radome as it seen in the Figure 4.39.

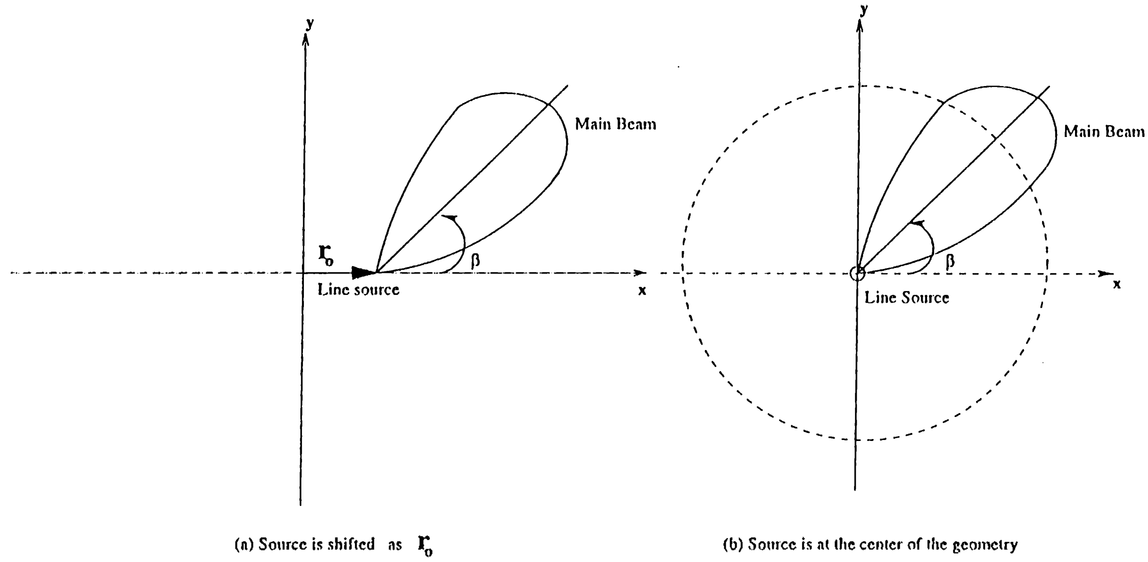

Figure 4.39: Position of the complex line source.

Directivity of the source can be found as

$$D = \frac{|E^{max}|^2}{\sum_n |a_n|^2} \tag{4.10}$$

where

$$a_n = j^n J_n(k_0 r_s) e^{-jn\phi_s} + j^{2n} J_n(k_0) c \sum_{m=1}^{M} C_{mn} e^{-jn\phi_m}. \tag{4.11}$$

If the source is at the center of the structure, $r_s = jb$, $\phi_s = \beta$ or if the source is shifted from the center as r_0, $r_s = \sqrt{r_0^2 - b^2 + 2jr_0 b cos\beta}$ and $\phi_s = cos^{-1}(\frac{r_0 + jbcos\beta}{r_s})$.

The Figure 4.40 and 4.41 show how the initial position of the source affects the power pattern. Here, $kc = 62.8$, $kb = 5$, $ka = 0.4$, $\beta = 180^0$ and $N = 5$. When the source is moved in backward direction of the beam, the distortions of the main beam decrease and the backscattered field decreases as well.

The Figures 4.42 and 4.43 present how the total field changes with the source position.

The directivity variations versus source position r_0 are presented in Figures 4.44 through 4.47 for both E and H polarization. For the E polarization, the superposition of the incident wave and scattered wave depend on the delay distance (distance between source and scatterer). When the delay distance is a multiple of λ, the interference is constructive; when it is an odd multiple of $\lambda/2$, the interference is destructive. The phase difference between H and E polarization is about 90^0.

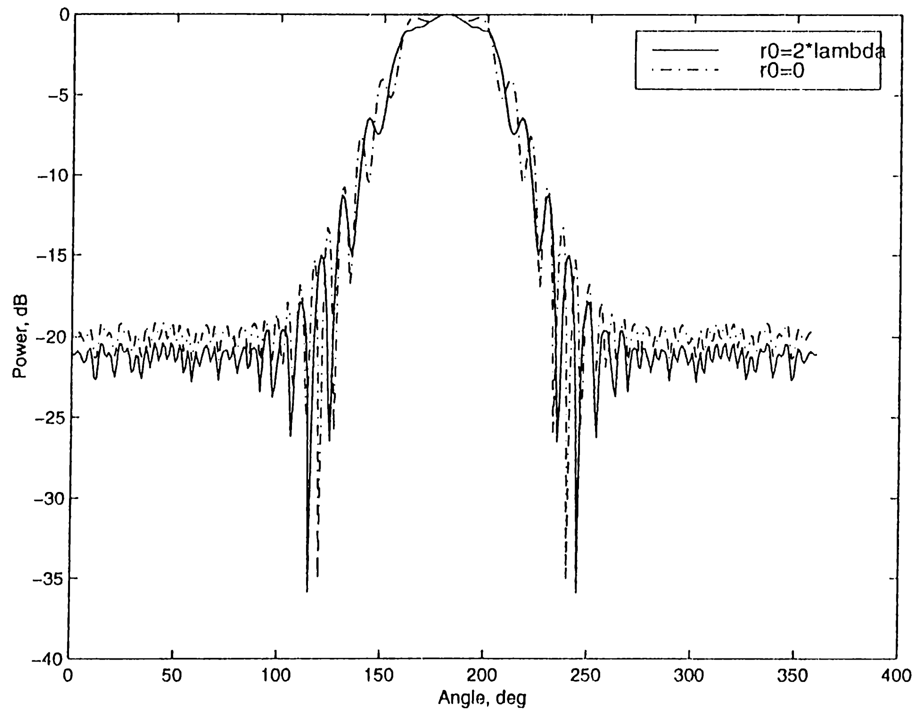

Figure 4.40: Power versus Angle (E polarization) for a grating consisting of four cylinders: kc=62.8, kb=5; ka=0.4, Beta=180 deg, N=5, r0=2lambda and r0=0.

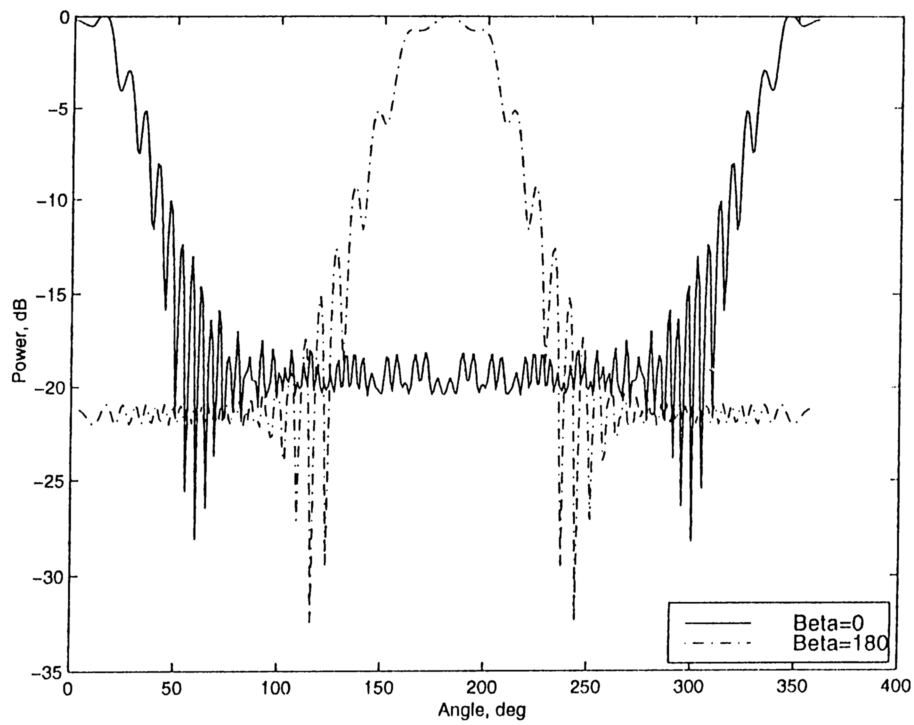

Figure 4.41: Power versus Angle for a grating consisting of four cylinders: kc=62.8, kb=5; ka=0.4, N=5, r0=2lambda.

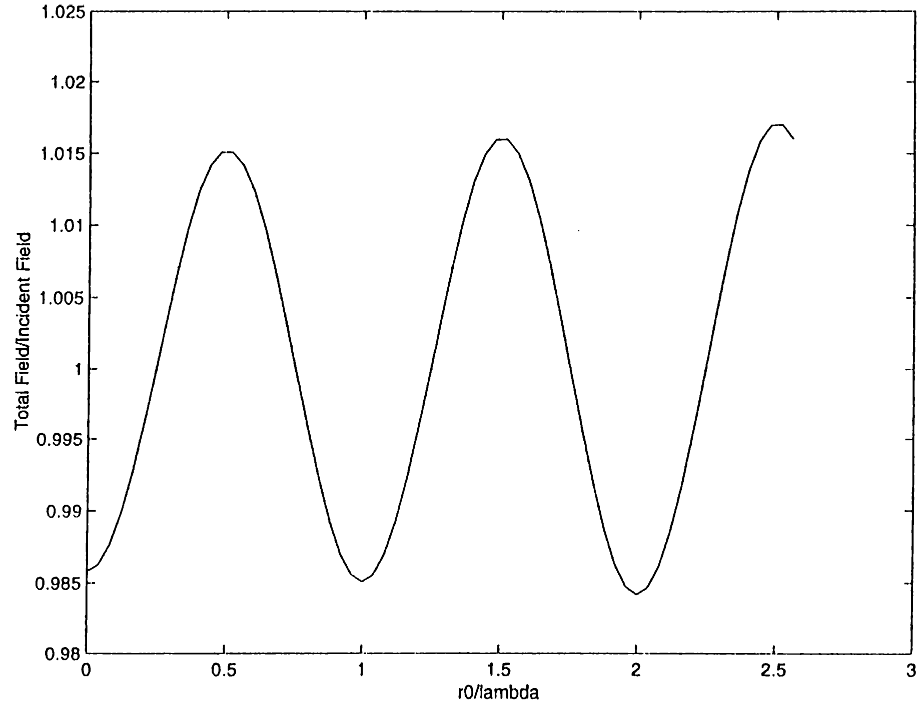

Figure 4.42: Total power versus r0 (E polarization)for a grating consisting of a single cylinders:M=1, kc=62.8, kb=5;ka=0.4, Beta=0 deg, N=5.

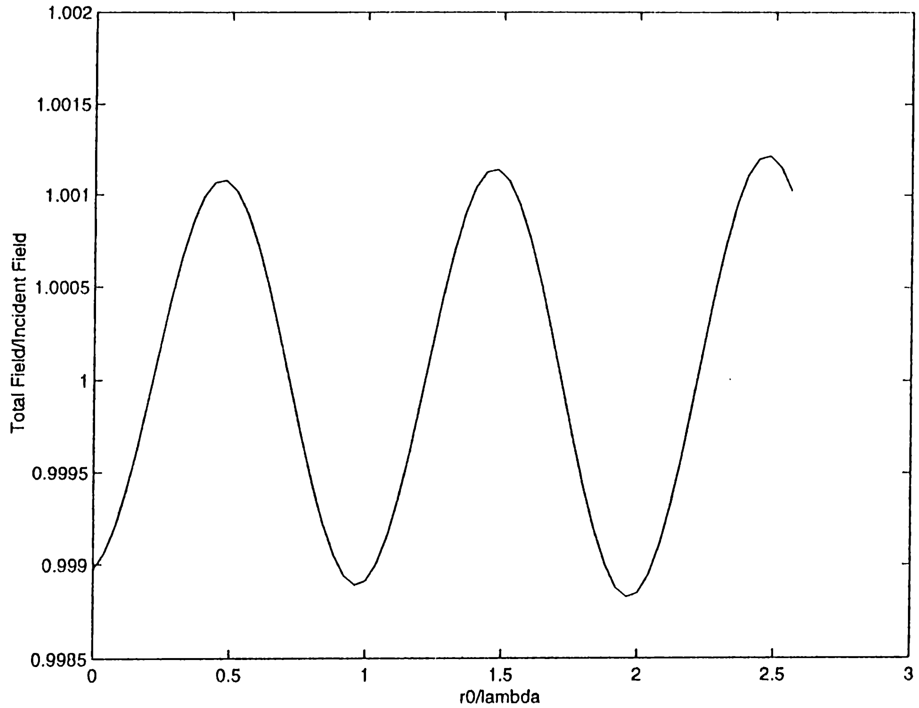

Figure 4.43: Total power versus source position (for E polarization) for a grating consisting of two cylinders:M=2, kc=62.8, kb=5; ka=0.4, N=5, r0=2lambda

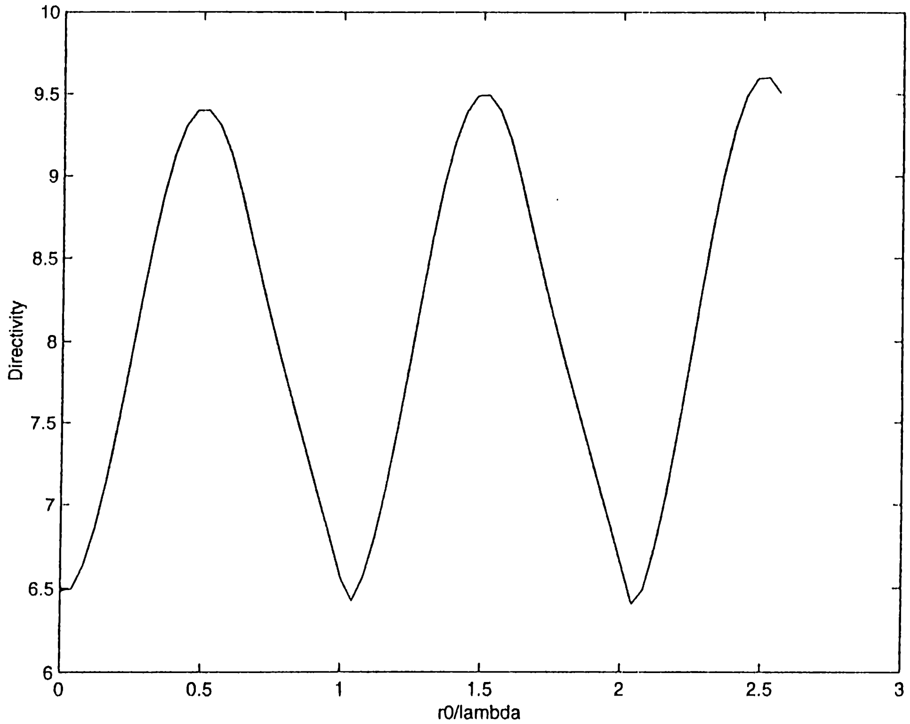

Figure 4.44: Directivity versus source position (for E polarization) for a grating consisting of a single cylinders: kc=62.8, kb=5;ka=0.4, Beta=0 deg, N=5

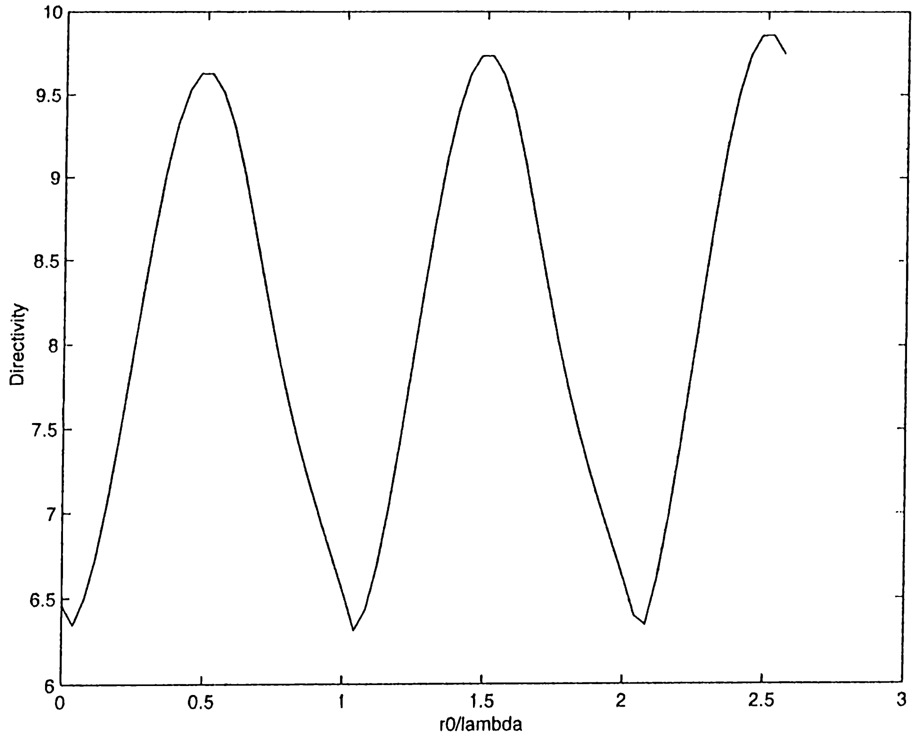

Figure 4.45: Directivity versus source position (for E polarization) for a grating consisting of two cylinders: M=2, kc=62.8, kb=5; ka=0.4, N=5.

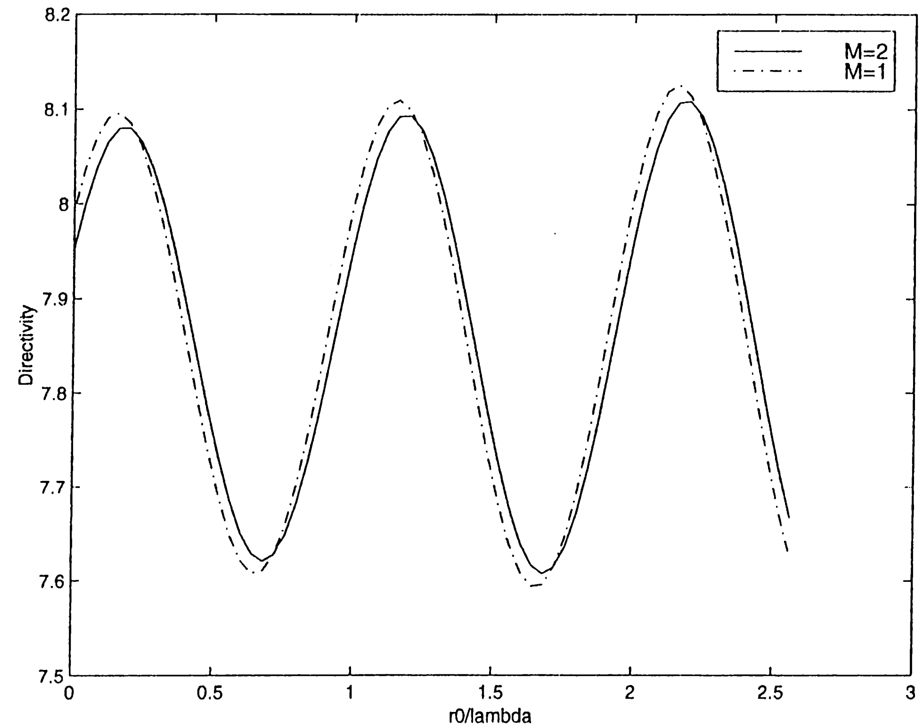

Figure 4.46: Directivity versus source position (for H polarization) for a grating consisting of one and two cylinders: kc=62.8, kb=5;ka=0.4, Beta=0 deg, N=5.

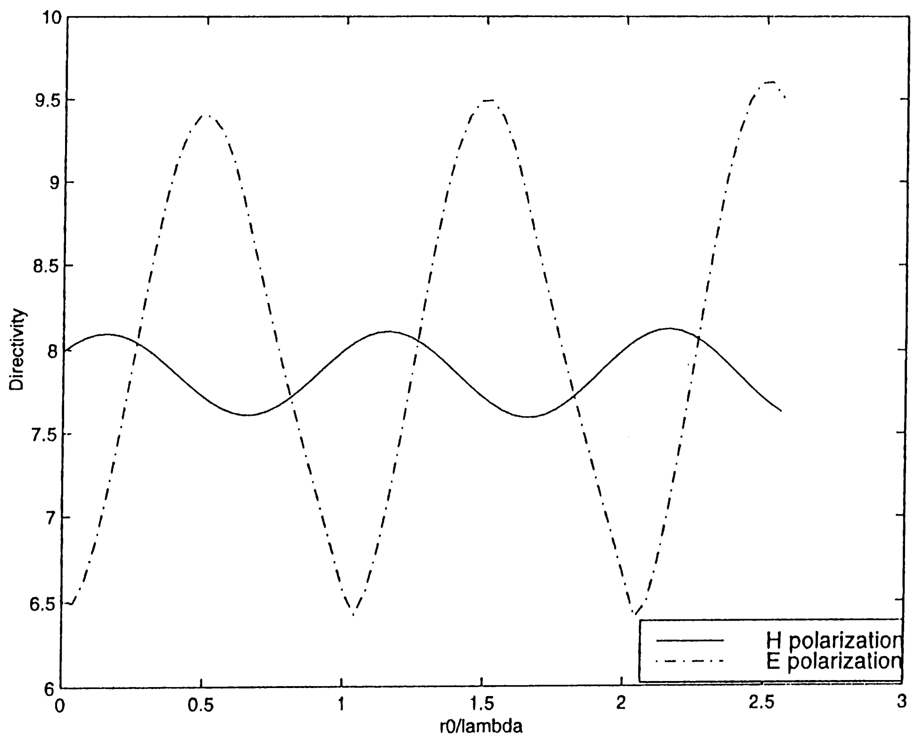

Figure 4.47: Directivity versus source position (for E and H polarizations) for a grating consisting of two cylinders:M=2, kc=62.8, kb=5; ka=0.4, N=5, r0=2lambda.

Chapter 5

CONCLUSIONS

In this thesis, the problem of electromagnetic wave penetrating through a circular radome with gratings consisting of an array of periodic perfectly conducting cylinders is considered. To the best of our knowledge, this is the first study made so far to such a problem with this approach. The far field in both polarizations is calculated canonically for real and complex line source surrounded by a grid structure. Extension to other types of excitations such as plane wave is straightforward and requires minimal changes in the analysis. The analysis is cast into a form which is simple for computations as well as in predicting the effect of mutual interactions between any number of cylinders. This technique is used for modeling two-dimensional scattering objects by using a number of parallel circular conducting cylinders. The validity and usefulness of the proposed method for modeling circular radome surrounded by conducting cylinders are presented by several examples.

The results for the normalized power pattern and the directivity are calculated numerically for various structure parameters and as a function of the observation angle and of the beam orientation. The directivity variations with beam direction are also presented. For the validation of methods, results are generated and compared with the available ones for simple geometries.

According to our numerical data, the distortion of the main beam increases, and the directivity decreases with increasing the number of cylinders and with increasing the radius of each cylinder. The distortion of the normalized power is decreased by increasing the radius of the grating. The directivity shows considerable variations as a function of the beam direction. It shows oscillations as a function of both the radome radius and the frequency of the source.

Bibliography

[1] Abdehamid Benali, Jean Chandezon, and Jacques Fontain. "A New Theory for Scattering of Electromagnetic Wave from Conducting or Dielectric Rough Surfaces". *IEEE Trans. Antennas Propagat.*, vol.40:141–147, 1992.

[2] Anil Bircan. *"A Study of Line Source Fields Transmitted Through a 2-D Circular Radome or a Slab"*. A master thesis submitted to Faculty of Engineering and Science of Bilkent University, 1996.

[3] Kevin Kample. *"Introduction to Radar Systems"*. 1986.

[4] D. C. F Nu and R. C. Rudduck. "Plane Wave Spectrum-Surface Integratioon Technique for Radome Analysis". *IEEE Trans. Antennas Propagat.*, vol.22:497–500, May 1974.

[5] Slim Quardani. *"Radiation Fields of a Complex Source in 2-D Circular Radome with Metal Gratings"*. A master thesis submitted to Faculty of Engineering and Science of Bilkent University, August 1997.

[6] Atef Z. Elsherbeni and Ahmed A. Kishk. "Modelling of Cylindrical Objects by Circular Dielctric and Conducting Cylinders". *IEEE Trans. Antennas Propagat.*, vol.40:97–100, 1992.

[7] J. W. Young and J. C. Bertron. "Multiple Scattering by Two Cylinders". *J.Acoust. Soc. of Amer.*, vol.58:1190–1195, 1975.

[8] Atef Z. Elsherbeni and M. Hamid. "Scattering by Parallel Conducting Circular Cylinders". *IEEE Trans. Antennas Propagat.*, vol.35:355–358, 1987.

[9] K. K. Mei and J. Van Bladel. "Scattering by Perfectly Conducting Rectangular Cylinder". *IEEE Trans. Antennas Propagat.*, vol.11:185–192, 1963.

[10] T. K. Wu and L. L. Tsai. "Scattering by Arbitrary Cross Sectioned Layered Lossy Dielectric Cylinders". *IEEE Trans. Antennas Propagat.*, vol.25:518–524, 1977.

[11] J. M. Jin and U. U. Liepa. "Application of Hybrid Finite Element Method to electromagnetic scattering From Coated Cylinders". *IEEE Trans. Antennas Propagat.*, vol.36:50–54, 1988.

[12] C. A. Balanis. *"Advanced Engineering Electromagnetics"*. John Wiley & Sons.

[13] Ehud Heyman and B. Z. Streinberg. "Complex Source". *IEEE Trans. Antennas Propagat.*, vol.38, 1990.

[14] Cornelis F. Du. Toit. "The Numerical Computation of Bessel Functions of the First and Second Kind for Integer Order and Complex Arguments". *IEEE Trans. Antennas Propagat.*, vol.38:1341–1349, 1990.